6

Wireless Powered Communications

6.1 Introduction

Wireless powered communications refer to the communications systems where the power of the communications device is supplied via wireless power transfer. This method is particularly useful for energy-constrained systems, such as a remote sensor or a mobile phone. In such systems, without wireless power transfer, when the battery is drained or the mains power is disconnected, the communications device will have to stop operations. Figure 6.1 shows some scenarios where wireless power can be used. In these cases, it is impossible or too costly to replace the battery of the device. Hence, wireless power transfer will be a good solution.

In general, energy harvesting wireless communications use different media to carry energy and information. For example, the communications device could harvest the solar power and then use the harvested solar power to send information via radio waves. One unique characteristic of wireless powered communications is that energy and information are often carried by the same wireless media. This saves the hardware cost.

There are many different sources of energy. There are also many different types of wireless systems. Thus, wireless powered communications can be implemented in different forms. For example, in Wang et al. (2015), wireless powered communications using lights have been discussed, where a solar panel was used to convert the solar power into electricity as an energy transducer. The same solar panel was also used as a photodetector to decode the modulated light signal for information. In Kisseleff et al. (2017), near-field magnetic induction was used to transmit data and wireless power at the same time. The inducted signal was split into several streams, one for data and the rest for power. By guaranteeing certain quality of service for data transmission, the total transferred power was maximized. One may also use sounds to transmit power and information simultaneously. However, the problem with lights and sounds is that they often require line-of-sight (LOS). The problem with near-field magnetic induction is that its efficiency drops very quickly as the distance increases. Due to these shortcomings, lights, sounds and magnetic induction have very limited applications. On the other hand, far-field radio frequency (RF) does not have these restrictions. It can penetrate walls or buildings through non-line-of-sight (NLOS) propagation, and it often covers distances of hundreds or thousands of meters. In this chapter, we will focus on wireless powered communications using far-field RF signals.

Energy Harvesting Communications: Principles and Theories, First Edition. Yunfei Chen.

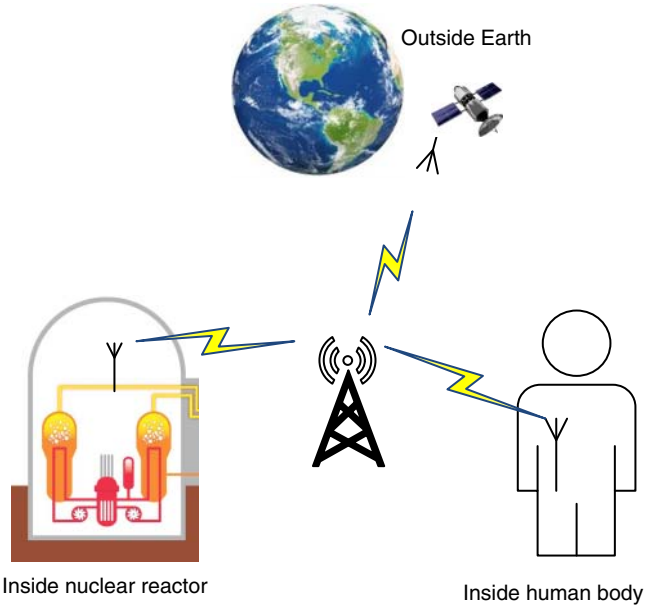

Figure 6.1 Some scenarios where wireless power is a promising alternative.

6.2 Types of Wireless Powered Communications

Since there are many different forms of wireless power in a communications system, it is useful to categorize them and then discuss them separately.

If the power transmitter has dedicated hardware for power transfer, this can be denoted as power beacon (PB)-based communications (Huang and Lau 2014). In this case, the PB is dedicated to power coverage in the network by broadcasting RF power, while the normal base stations still provide information coverage. If the power transmitter shares the hardware with the information transmitter, power transfer and information delivery can happen in different time slots. This can be denoted as hybrid access point (HAP)-based communications (Ju and Zhang 2014). In this case, the same transmitter will be used for power transfer during some periods of time and for information delivery during other periods of time. If the power transmitter and the information transmitter not only share the hardware but also operate in the same time slot, this can be denoted as simultaneous wireless information and power transfer (SWIPT). In SWIPT, the receiver splits the received signal into two parts in either the time domain or the power domain, one part for power reception and the other part for information reception. Figure 6.2 compares these three types. Note that they differ in the way wireless power is transferred. In the following sections, these three different forms will be discussed in detail.

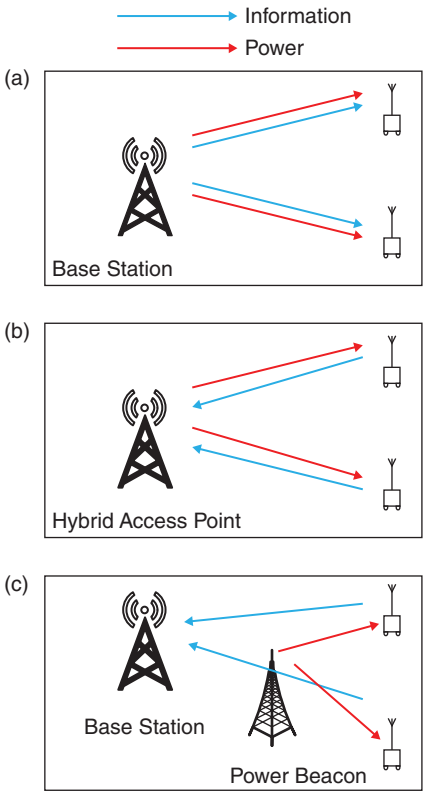

Figure 6.2 Different types of wireless powered communications: (a) SWIPT; (b) HAP; and (c) PB.

6.3 Simultaneous Wireless Information and Power Transfer

SWIPT is probably the earliest form of wireless powered communications that has been proposed in the literature. For a simple wireless power transfer circuit using magnetic induction, it can be proven that the power transfer efficiency is maximized at a specific frequency, or using a single sinusoid (Grover and Sahai 2010). However, according to Shannon's theorem, the information rate for a single sinusoid is zero, because its bandwidth is zero. For this reason, in the past few decades, messages and power have been transmitted using separate signals to maximize both the information rate and energy rate. Hence, we have power engineers working on power transfer and communications engineers working on message transmission. Two separate infrastructure networks have been designed: an electricity grid dedicated to power transfer; and communications networks dedicated to message transmission. It is reasonable to combine these two networks to save costs by using the same signal in the same network to transmit both power and information. In order to do this, a tradeoff between information rate and power transfer efficiency has to be made. This is the motivation of most recent studies on SWIPT.

6.3.1 Ideal Implementations

Several information theoretic studies were conducted in Varshney (2008) and Grover and Sahai (2010) to find for the first time the fundamental tradeoff between transmitting message and transmitting energy over a single noisy line. This tradeoff aims to optimize the energy rate and the information rate of the same signal at the same time.

Specifically, in Varshney (2008), a capacity-energy function is constructed by maximizing the mutual information under the constraint of a minimum received power. The optimization problem can be described as

$$C(B) = \max_{X:E[b(Y)]\geq B} I(X,Y) \tag{6.1}$$

where a discrete memoryless channel is considered, X is the input to the channel, Y is the output of the channel, $I(X,Y)$ is the mutual information between input and output, $b(Y)$ is the energy of the output Y, $E[b(Y)]$ is the average energy defined as $E[b(Y)] = \sum_{Y\in\mathbb{Y}} b(Y)p(Y)$, $\mathbb{Y}$ is the output alphabet, $p(Y)$ is the probability of Y, $0 \leq B \leq B_{max}$, B_{max} is the maximum element of $\mathbf{b}^T\mathbf{Q}$, $\mathbf{b}$ is a column vector of $b(Y)$ with all possible outputs in $\mathbb{Y}$, and $\mathbf{Q}$ is the transition probabilities between inputs in the input alphabet $\mathbb{X}$ and outputs in the output alphabet $\mathbb{Y}$. Several properties of $C(B)$ have been reported in Varshney (2008). Similar results are also applicable to a continuous Gaussian channel.

The optimum value can be found by using the above equation as a rate-energy tradeoff in most cases. Varshney (2008) has given an example for a particular binary symmetric channel with crossover probability of p. In this case, the capacity-energy function can be shown as

$$C(B) = \begin{cases} \log(2) - h_2(p), & 0 \leq B \leq \frac{1}{2} \\ h_2(B) - h_2(p) & \frac{1}{2} \leq B \leq 1-p \end{cases} \tag{6.2}$$

where $h_2(\cdot)$ is the binary entropy function. Figure 6.3 shows $C(B)$ versus B in (6.2). This function is not a continuous function. Several other examples have also been given in Varshney (2008). Interested readers are referred to Varshney (2008) for more details.

Grover and Sahai (2010) studied another tradeoff between power transfer and information rate by using the same signal. Recognizing the fact that the power transfer circuit is a frequency-selective channel, this study aims to maximize the total information rate

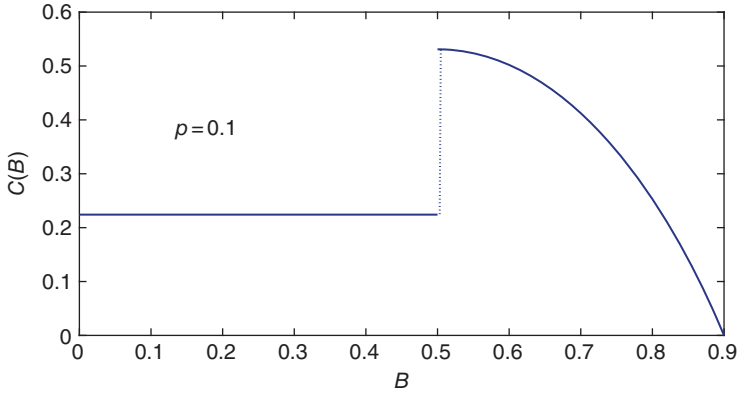

Figure 6.3 $C(B)$ versus B in (6.2).

subject to one constraint on the total power available at the transmitter and another constraint on the total transferred power at the receiver. Specifically, the output voltage of the receiver can be expressed as

$$V_{o,i} = h_i \sqrt{R_r} I_{s,i} + Z_i \tag{6.3}$$

where i indexes the ith frequency band by dividing the total bandwidth into N parts such that each band is narrow-band frequency-non-selective channel (the channel is frequency-selective across the whole bandwidth of $\sum_{i=1}^{N} f_i$), h_i is the transfer function of the ith band at frequency f_i, R_r is the load at the receiver, $I_{s,i}$ is the amplitude of the input current at the ith band so that the current through the receiver load is $h_i I_{s,i}$, and Z_i is the additive white Gaussian noise.

The average power consumed over the internal resistance R_s at the transmitter is $P_{s,i} = E[|I_{s,i}|^2]R_s$, where $E[|I_{s,i}|^2]$ is the average over the random messages. The average power consumed at the load in the receiver is $P_{r,i} = E[|I_{s,i}|^2]|h_i|^2 R_r$. Thus, the total power in the ith band available at the transmitter is $P_i = E[|I_{s,i}|^2](R_s + |h_i|^2 R_r)$, including both power consumed at the transmitter and the power delivered to the receiver. Using P_i, one has $P_{r,i} = \eta_i P_i$, where $\eta_i = \frac{|h_i|^2 R_r}{R_s + |h_i^2| R_r}$ is the power transfer efficiency of the ith band.

Denote P_A as the total power available at the transmitter and P_B as the total power that is required to be delivered to the receiver. The optimization problem can be described as

$$C(P_A, P_B) = \max_{P_i : \sum_{i=1}^{N} P_i \le P_A, \sum_{i=1}^{N} \eta_i P_i \ge P_B} \left\{ \sum_{i=1}^{N} \log_2 \left(1 + \frac{\eta_i P_i}{W} \right) \right\} \tag{6.4}$$

where W is the noise power.

Thus, from (6.4), the sum rate is maximized by optimizing the power allocation across different bands, subject to the total transmitted power and the total delivered power constraints.

The maximum sum rate follows the water-filling algorithm. The optimal solution to (6.4) is given by

$$C(P_A, P_B) = \sum_{i=1}^{N} \log_2 \left(1 + \frac{\eta_i P_i^{opt}}{W} \right) \tag{6.5}$$

where $P_i^{opt} = \max\{ \frac{\log_2(e)}{\lambda^{opt} - \eta_i \mu^{opt}} - \frac{W}{\eta_i}, 0 \}$ is the optimum power that should be allocated to the ith band, $\max\{\cdot, \cdot\}$ takes the maximum of two values, and the parameters λ^{opt} and μ^{opt} satisfy the two equations

$$\sum_{i=1}^{N} \max \left\{ \left(\frac{\log_2(e)}{\lambda^{opt} - \eta_i \mu^{opt}} - \frac{N}{\eta_i} \right), 0 \right\} = P_A \tag{6.6}$$

$$\sum_{i=1}^{N} \eta_i \max \left\{ \left(\frac{\log_2(e)}{\lambda^{opt} - \eta_i \mu^{opt}} - \frac{N}{\eta_i} \right), 0 \right\} = P_B. \tag{6.7}$$

A continuous version of this optimization was also discussed in Grover and Sahai (2010), where η_i is replaced by $\eta(f)$, the power transfer efficiency as a function of frequency, and summation is replaced by integration over frequency.

Comparing (6.1) with (6.4), one sees that (6.1) imposes a constraint on the average transferred power, while (6.4) imposes a constraint on the total transmitted power and a

constraint on the total transferred power. Thus, they lead to different solutions. Another difference between them is that (6.4) considers the frequency selectivity of the channel while (6.1) does not. However, both of them aim to maximize the information rate. Alternatively, one can also maximize the transferred power subject to constraints on the information rate. Other variants are also possible and may be useful in different applications.

6.3.2 Practical Implementations

The information theoretic bounds give the limiting performances of SWIPT. However, these bounds are only theoretically possible. In practice, it is difficult to use the same signal for both power transfer and information decoding at the same time, as the signal used for information decoding cannot be harvested for energy again, and vice versa. The results in Grover and Sahai (2010) and Varshney (2008) have assumed that one can use the signal for energy harvesting and then use the same signal again for information decoding. Thus, practical schemes for SWIPT are needed.

Such practical designs were first discussed in Zhang and Ho (2013) and Zhou et al. (2013b). In the following, Zhou et al. (2013b) will be used to explain how these practical designs work. We will focus on the separated information and energy receiver case in Zhou et al. (2013b), as the integrated information and energy receiver case in Zhou et al. (2013b) has certain limitations.

Since energy and information carried by the same signal cannot be processed at the same time, practical SWIPT implementations solve this problem in a simple way by splitting the signal into two parts: one part for power transfer or energy harvesting; and the other part for message transmission or information decoding. Thus, one has two main methods of SWIPT: time switching (TS) and power splitting (PS). Figure 6.4 compares these two methods. Generally speaking, TS splits the signal in the time domain, while PS splits the signal in the power domain. Their principles are explained in detail in the following.

6.3.2.1 Time Switching

For TS, the signal is split in the time domain. A switch is used such that during one part of the transmission time the received signal is connected to an energy harvester for power transfer and during the other part of the transmission time the received signal is switched to an information decoder for message delivery. Thus, the most important design parameter in this method is called the time-switching coefficient. The switching can happen within one packet between its data part and energy part, or between packets, depending on whether the whole packet or only part of the packet is used for power transfer. Without loss of generality, one can assume that the total transmission time is T seconds, of which αT seconds are used for power transfer and $(1-\alpha)T$ seconds are used for information delivery, where $0 \le \alpha \le 1$ is the TS coefficient. The time T could be the symbol, frame or packet interval. Thus, the signal received for processing can be expressed as

$$y(t) = \begin{cases} h\sqrt{P_s}s(t) + n(t), & 0 \le t \le \alpha T \\ h\sqrt{P_s}s(t) + n(t) & \alpha T \le t \le T \end{cases} \tag{6.8}$$

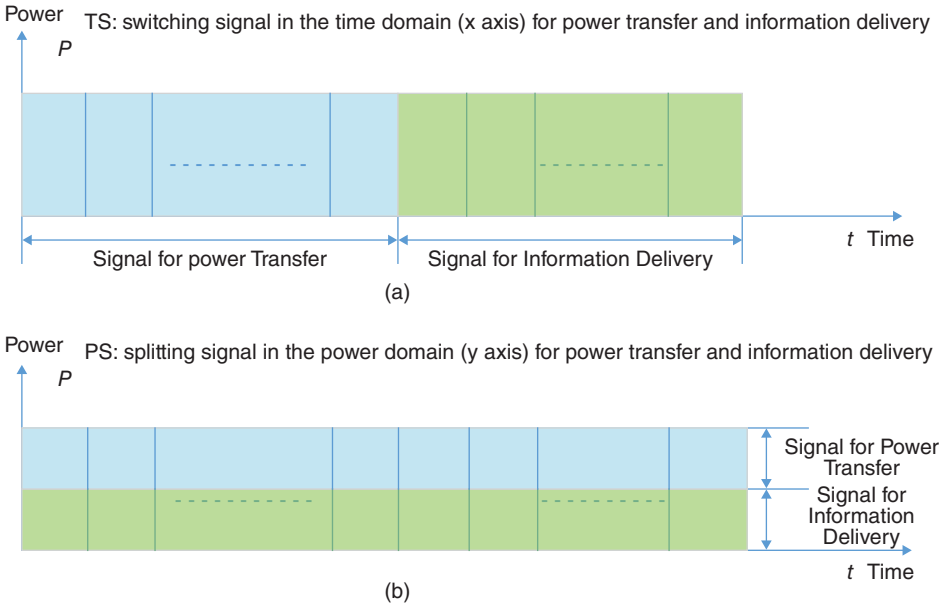

Figure 6.4 Comparison of (a) TS and (b) PS.

where P_s is the transmission power, $s(t)$ is the transmitted data symbol or any symbol, h is the complex channel gain between the transmitter and the receiver and $n(t)$ is the complex additive white Gaussian noise (AWGN) with mean zero and variance $2\sigma^2$. Note that this model is a baseband model where the signal has already been down-converted and the in-phase and quadrature components have been combined. From (6.8), the first part is used for energy harvesting to give the total harvested energy as

$$E = \eta\alpha P_s|h|^2 T \tag{6.9}$$

where η is the conversion efficiency of the harvester, which has been discussed in Chapter 3. Also, $E[|s(t)|^2] = 1$ has been assumed so that all the transmitted symbols have unit power. The second part is used for information decoding, and its achievable rate is given by

$$C = (1-\alpha)\log_2\left(1 + \frac{P_s|h|^2}{2\sigma^2}\right) \tag{6.10}$$

where $(1-\alpha)$ takes the penalty of power transfer into account (αT could have been used for data transmission for higher information rates). As can be seen from (6.9) and (6.10), a larger value of α gives more harvested energy but at the same time reduces the information rate. This tradeoff can be best described by using the rate-energy function defined in Zhou et al. (2013b) as

$$C(R,Q) = \left\{ Q \le \alpha\eta P_s|h|^2, R \le (1-\alpha)\log_2\left(1 + \frac{P_s|h|^2}{2\sigma^2}\right)\right\} \tag{6.11}$$

where $\alpha\eta P_s|h|^2$ is the harvested energy (the term power and the term energy are used interchangeably in this chapter). Figure 6.5 shows the rate-energy function for TS. Note

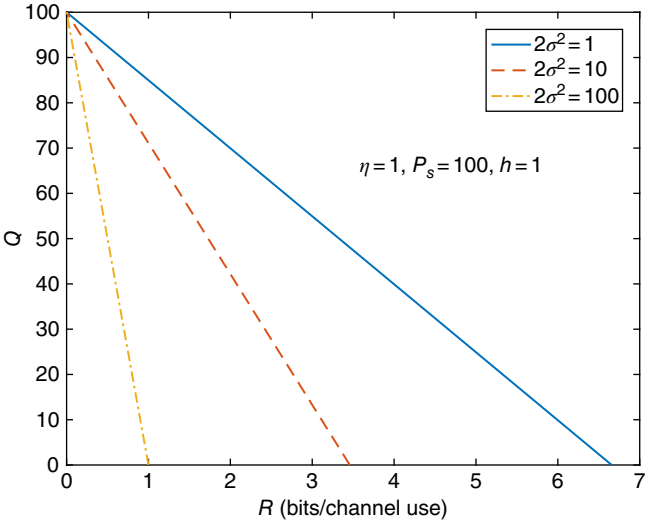

Figure 6.5 The rate-energy function for TS.

that the straight line is only the boundary and the actual rate-energy region is below the straight line. One sees that the rate-energy region increases when the noise power decreases, or when the signal-to-noise ratio (SNR) increases. The maximum rate or the maximum power can be achieved at the two ends of this straight line. On the other hand, if there is any constraint on rate or power, the optimum point will be somewhere between these two end points. This function is essentially the same as $C(B)$ studied in Varshney (2008) and $C(P_A, P_B)$ studied in Grover and Sahai (2010), only in a different form. Remember that we started from the fact that power transfer efficiency and information rate cannot be maximized at the same time and hence, we look for a tradeoff between them.

6.3.2.2 Power Splitting

For PS, the signal is split in the power domain. A power splitter is used in the circuit so that the received signal as an input will be divided into two parts: one part is fed into the energy harvester for energy harvesting and the other part is fed into the decoder for information decoding. Thus, unlike TS, energy harvesting and information decoding can be processed simultaneously but separately. The most important design parameter in this case is the PS factor, similar to the TS coefficient. Thus, the received signals for power transfer and for information delivery, respectively, can be written as

$$y_1(t) = \sqrt{\rho P_s} hs(t) + \sqrt{\rho} n_a(t) + n_d(t), \ 0 \le t \le T \tag{6.12a}$$

$$y_2(t) = \sqrt{(1-\rho) P_s} hs(t) + \sqrt{1-\rho} n_a(t) + n_d(t), \ 0 \le t \le T \tag{6.12b}$$

where ρ is the PS factor, $n_a(t)$ is the complex AWGN introduced by the antenna with mean zero and variance $2\sigma_a^2$, and $n_d(t)$ is the complex AWGN introduced by the conversion with mean zero and variance $2\sigma_d^2$. Again, this is a baseband signal model.

Several observations can be made. First, $n(t)$ in (6.8) is related to $n_a(t)$ and $n_d(t)$ in (6.12a,b) as $n(t) = n_a(t) + n_d(t)$. In other words, the AWGN in (6.8) actually consists

of noise from the antenna as well as noise from processing. Thus, $2\sigma^2 = 2\sigma_a^2 + 2\sigma_d^2$. Secondly, the power splitting is applied to the received RF signal. Thus, one has $\sqrt{\rho}n_a(t)$ and $\sqrt{1-\rho}n_a(t)$, as $n_a(t)$ is part of the RF signal and is also split.

Using (6.12a,b), the total energy harvested from the energy signal is given by

$$E = \eta\rho P_s|h|^2 T \tag{6.13}$$

and the achievable rate of the information signal is given by

$$C = \log_2\left[1 + \frac{(1-\rho)P_s|h|^2}{(1-\rho)2\sigma_a^2 + 2\sigma_d^2}\right]. \tag{6.14}$$

Unlike TS, there is no penalty of power transfer in terms of information rate, as energy harvesting and information decoding are processed simultaneously. Thus, it has been shown in many studies that PS can provide a higher data rate than TS, under the same other conditions. As can be seen from (6.13) and (6.14), when ρ increases, more power can be harvested but the information rate decreases. Using the rate-energy function defined in Zhou et al. (2013b), this tradeoff is given as

$$C(R,Q) = \left\{ Q \le \eta\rho P_s|h|^2, R \le \log_2\left[1 + \frac{(1-\rho)P_s|h|^2}{(1-\rho)2\sigma_a^2 + 2\sigma_d^2}\right]\right\}. \tag{6.15}$$

Figure 6.6 gives an example of the rate-energy function for PS. Again, the line represents the boundary of the rate-energy region. Unlike TS, in this case, the boundary for PS is not a straight line and it is actually a convex function. Thus, PS has a larger rate-energy region. It can be shown that PS and TS have the same maximum power and maximum rate or the same end points for the curves, under the same conditions, but for a tradeoff between the two end points, PS normally has a larger power or rate than TS. This tradeoff is the same tradeoff as what we are looking for in TS and in Grover and Sahai (2010)

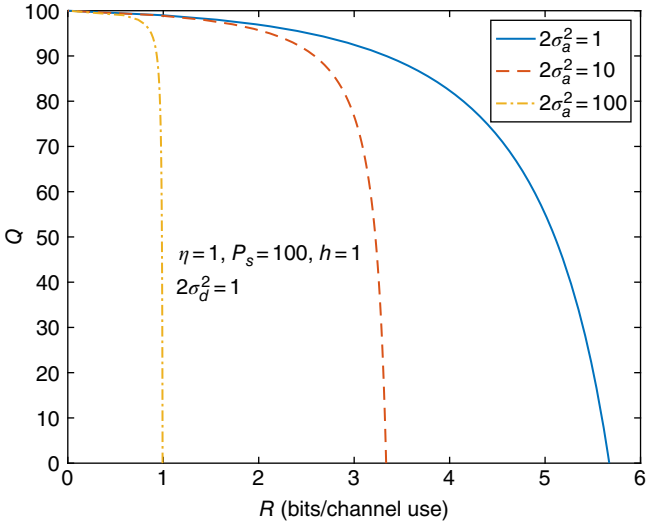

Figure 6.6 The rate-energy function for PS.

and Varshney (2008). In fact, most studies on SWIPT have been conducted to find this tradeoff under different conditions, such as multiple antennas, joint designs of power allocation and scheduling, etc. Some examples will be given later.

6.3.2.3 General Scheme

Although not necessary, it is useful to unify TS and PS to have a better view of how they operate. In Zhou et al. (2013b), TS and PS were unified under dynamic power splitting (DPS). Specifically, denote ρ_k as the PS factor for the kth symbol, frame, or packet. Following a similar procedure as before, the harvested energy can be derived as

$$E_k = \eta \rho_k P_s |h|^2 T \tag{6.16}$$

and the achievable rate is

$$C_k = \log_2 \left[1 + \frac{(1-\rho_k) P_s |h|^2}{(1-\rho_k) 2\sigma_a^2 + 2\sigma_d^2} \right]. \tag{6.17}$$

Considering the average harvested power and the average rate, for K symbols, frames, or packets, the rate-energy function is

$$C(R,Q) = \left\{ Q \le \frac{\eta P_s |h|^2}{K} \sum_{k=1}^{K} \rho_k, R \le \frac{1}{K} \sum_{k=1}^{K} \log_2 \left[1 + \frac{(1-\rho_k) P_s |h|^2}{(1-\rho_k) 2\sigma_a^2 + 2\sigma_d^2} \right] \right\}. \tag{6.18}$$

For TS discussed before, using the model of DPS, one has

$$\rho_k = \begin{cases} 1, & k = 1, 2, \cdots, \alpha K \\ 0, & k = \alpha K + 1, \alpha K + 2, \cdots, K \end{cases} \tag{6.19}$$

and for PS discussed before, one has

$$\rho_k = \rho, \quad k = 1, 2, \cdots, K. \tag{6.20}$$

It can be verified that, if one uses (6.19) and (6.20) in (6.18), one can obtain (6.11) and (6.15), respectively. Figure 6.7 shows a diagram that unifies TS and PS under the same structure. In this figure, $n(t)$ is $n_a(t)$ for PS, as $n_d(t)$ will only occur inside the information decoding box or the energy harvesting box. There are other forms of SWIPT implementation. For example, one can combine TS with PS so that a time switcher is first used to obtain dedicated power transfer time and then a power splitter is used during the information delivery time to split the signal into two parts for energy harvesting and information decoding. These variants are not discussed here. It was further proved in Zhou et al. (2013b) that the PS scheme provides the best tradeoff between energy and information among these schemes. The only shortcoming of PS is that the hardware

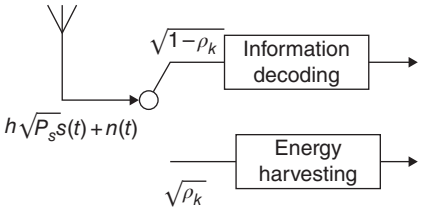

Figure 6.7 A unified structure for TS and PS.

implementation of a power splitter is much more complicated than a time switcher. Hence, one has to take both performance and complexity into account when choosing these SWIPT schemes.

Another issue that often causes confusion is that, in the above discussion and in most literature, the noise power is ignored in energy harvesting. Thus, in (6.9), (6.13), and (6.16), only the energy of the signal part is accounted for. This is based on the assumption that the noise is normally much weaker than the signal. If the noise is comparable with the signal, then the noise power can be added back in (6.9), (6.13), and (6.16), as it is part of the received energy. In addition to PS and TS, other SWIPT techniques can also be used. For example, antenna switching that splits a subset of antennas for information and another subset of antennas for energy was proposed in Ben Khelifa and Alouini (2017a) and Ben Khelifa et al. (2017). This splits the received signal in the space domain.

6.4 Hybrid Access Point

HAP is another useful form of wireless powered communications (Ju and Zhang 2014). The definition of HAP comes from the fact that the access point or the base station in this network serves as both a power transmitter and an information transmitter and so is hybrid. In most applications, the function of power transmitter and the function of information transmitter are performed at the HAP in a time-division-duplex (TDD) manner, as frequency-division-duplex would lead to extra costs at both the HAP and the remote device. In this case, as will be shown later, HAP is theoretically very similar to the TS scheme in SWIPT. Figure 6.8 shows a HAP wireless powered communications system with one HAP and K nodes. SWIPT is suitable for point-to-point wireless powered communications, while HAP is suitable for point-to-multi-point wireless powered communications.

6.4.1 Rate-Energy Tradeoff

Consider a HAP wireless powered communications system, where one HAP serves K remote devices. The TDD protocol proposed in Ju and Zhang (2014) is adopted,

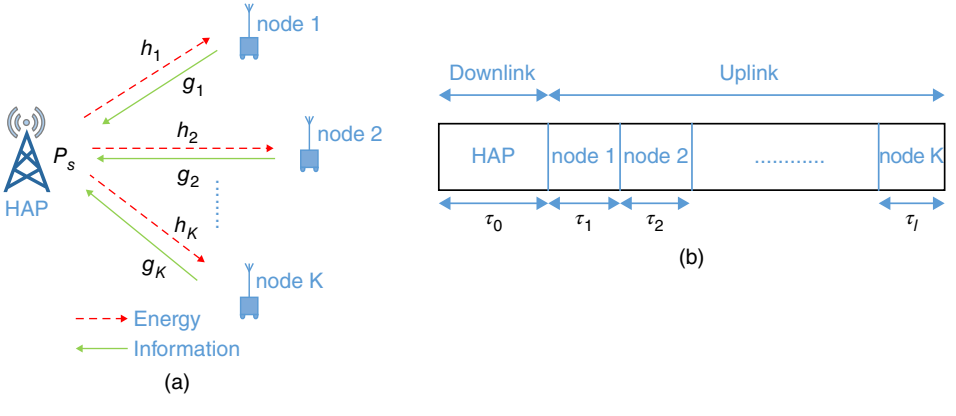

Figure 6.8 HAP wireless powered communications: (a) HAP structure; and (b) HAP link time.

where the HAP broadcasts wireless power in the downlink for τ_0 seconds, followed by information transmission from the nodes to the HAP in the TDD uplink using the harvested energy. Denote τ_k as the transmission time of node k, where $k = 1, 2, \cdots, K$. The fundamental tradeoff between energy and information occurs when the total time $\tau_0 + \sum_{k=1}^{K} \tau_k = T$ is fixed. Thus, if one increases τ_0 or the power transfer time, more energy can be harvested by the nodes such that they can use a larger transmission power for the information transmission in the uplink, while the information transmission time will be reduced such that less data symbols can be sent. Thus, unlike SWIPT where the tradeoff between energy and information is considered for the use of the same signal, HAP considers this tradeoff for the use of the same link. If one lets $K = 1$, one can easily see that this problem is very similar to the TS scheme in SWIPT. Next, assume that the received signal in the downlink is given by

$$y_k = h_k \sqrt{P_s} s + n_k \tag{6.21}$$

where $k = 1, 2, \cdots, K$, h_k is the complex channel gain from the HAP to the kth node, P_s is the transmission power of the HAP, s is the transmitted symbol and n_k is the complex AWGN at the kth node with mean zero and variance $2\sigma^2$. This signal is used for energy harvesting to give the harvested energy as

$$E_k = \eta P_s |h_k|^2 \tau_0. \tag{6.22}$$

The harvested energy is then used to transmit the information from the kth node to the HAP during τ_k as

$$r_k = g_k \sqrt{P_k} s_k + z_k \tag{6.23}$$

where g_k is the complex channel gain from the kth node to the HAP, s_k is the data symbol transmitted, z_k is the complex AWGN at the HAP during τ_k with mean zero and variance $2\sigma^2$, and P_k is the transmission power of the kth node given by

$$P_k = \frac{E_k}{\tau_k} = \eta P_s |h_k|^2 \frac{\tau_0}{\tau_k}. \tag{6.24}$$

Thus, the achievable information rate for the kth node is

$$R_k = \tau_k \log_2 \left(1 + \frac{P_k |g_k|^2}{2\sigma^2}\right) = \tau_k \log_2 \left(1 + \frac{\eta |g_k|^2 |h_k|^2 P_s \tau_0}{2\sigma^2 \tau_k}\right). \tag{6.25}$$

Note that the penalty τ_k must be added to account for the fact that only τ_k seconds are used by the kth node for information transmission.

In the derivation of (6.25), several assumptions have been made. First, it is assumed that all the harvested energy is used for transmission. This is the "harvest-then-transmit" protocol. It is possible to use only part of the harvested energy, if there is some energy storage device at the remote device. However, for sensor networks, this may not be necessary or possible. Secondly, all the energy loss has been ignored during the processing, except the conversion loss at the energy harvester represented by η. Thirdly, perfect synchronization is essential for this scheme, in fact, for all TDD protocols. Finally, h_k and g_k are random variables but only change from one transmission to the other. They remain constant during one transmission. Thus, block fading is assumed.

It can be shown that the rate in (6.25) increases with τ_0 for fixed τ_k, as more energy will be harvested for information transmission. It can also be shown that the rate in (6.25)

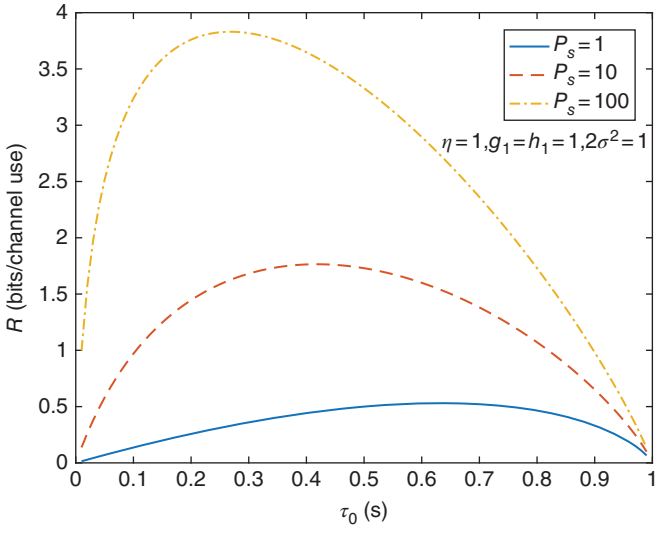

Figure 6.9 R_1 versus τ_0 when there is one node.

increases with τ_k for fixed τ_0, as more transmission time will be provided for information delivery. However, when the total time is fixed such that τ_0 and τ_k cannot increase at the same time, an optimal tradeoff exists. Figure 6.9 shows this tradeoff when there is only one node. It can be seen that an optimum value of τ_0 exists that maximizes the information rate. This optimization changes when P_s or the SNR changes.

The sum rate is obtained by adding the rates of all K devices to give

$$R(\tau_0, \cdots, \tau_K) = \sum_{k=1}^{K} R_k = \sum_{i=1}^{K} \tau_k \log_2 \left(1 + \frac{\eta |g_k|^2 |h_k|^2 P_s \tau_0}{2\sigma^2 \tau_k}\right). \tag{6.26}$$

Thus, the rate-energy function to be optimized in this system is

$$\begin{aligned} &\max_{\tau_0, \cdots, \tau_K} \{R(\tau_0, \cdots, \tau_K)\} \\ &s.t. \sum_{k=1}^{K} \tau_k \leq T \\ &\tau_k \geq 0, k = 1, 2, \cdots, K. \end{aligned} \tag{6.27}$$

Using the Lagrange multiplier, this optimization problem can be solved to give the optimum time intervals as

$$\tau_k^{opt} = \begin{cases} \frac{a_{opt}-1}{A+a_{opt}-1}, & k = 0 \\ \frac{\gamma_k}{A+a_{opt}-1} & k = 1, 2, \cdots, K \end{cases} \tag{6.28}$$

where $A = \sum_{k=1}^{K} \gamma_k$, T has been set to 1 for convenience,

$$\gamma_k = \frac{\eta |h_k|^2 |g_k|^2 P_s}{2\sigma^2} \tag{6.29}$$

is the SNR of the kth node, and a_{opt} is the solution to the equation $A = a \ln a - a + 1$. Thus, the maximum sum rate is given by

$$R_{max} = \sum_{i=1}^{K} \tau_k^{opt} \log_2 \left(1 + \frac{\eta |g_k|^2 |h_k|^2 P_s \tau_0^{opt}}{2\sigma^2 \tau_k^{opt}} \right). \tag{6.30}$$

One sees that, in order to achieve this optimum rate, knowledge of the channel gains h_k and g_k is required at the beginning of each transmission, based on which the time intervals will be allocated. Thus, this scheme is suitable for quasi-fading channels where h_k and g_k change slowly.

6.4.2 Fairness Issue

The time allocation in Section 6.4.1 gives the best tradeoff between energy and information for the link. However, it is not fair to all devices. To see this, one notes from (6.28) that the length of time interval allocated to the kth device is proportional to the SNR of the device γ_k. From (6.29), the SNR increases with the channel gains h_k and g_k. In a wireless communication channel, the channel gains increase when the distance between the transmitter and the receiver decreases (Stuber 2001). Thus, nodes closer to the HAP have larger channel gains for both h_k and g_k. Consequently, they will be allocated a longer transmission time, which is not fair to other nodes. This is called the doubly near-far problem in Ju and Zhang (2014).

To tackle this fairness problem, another sum rate optimization problem can be formulated as

$$\begin{aligned} &\max_{\tau_0, \cdots, \tau_K, R_0} \{R(\tau_0, \cdots, \tau_K)\} \\ &s.t. \sum_{k=1}^{K} \tau_K \le T \\ &\tau_k \ge 0, k = 1, 2, \cdots, K. \\ &R_k \ge R_0, k = 1, 2, \cdots, K. \end{aligned} \tag{6.31}$$

where an additional constraint has been added to make sure each node has at least a guaranteed minimum rate of transmission. This optimization does not have any analytical solution but can be solved iteratively. Interested readers are referred to Ju and Zhang (2014) for the detailed procedure.

6.4.3 Channel Knowledge Issue

Another issue related to the energy-rate tradeoff in the HAP wireless powered communications is the channel knowledge. As mentioned before, one needs to predict h_k and g_k for the next transmission in order to allocate the time intervals beforehand. This prediction seems not to be reliable in a dynamic wireless channel. Also, this knowledge needs to be updated frequently if the channels change fast. The overhead incurred by the prediction may not be tolerable in this case.

To avoid these issues, instead of using the rate in (6.25), one can average it over the channel gains h_k and g_k and then try to optimize the average sum rate. In the following, the average rate is obtained, which can be used in the optimization of (6.27) or (6.31).

It has already been shown in Section 6.4.1 that the achievable rate of the kth device is

$$R_k = \tau_k \log_2(1+\gamma_k) = \tau_k \log_2\left(1+\frac{\eta P_s \tau_0}{2\sigma^2\tau_k}|g_k|^2|h_k|^2\right). \tag{6.32}$$

Similarly, the bit error rate (BER) of the kth device is

$$B_k = \frac{1}{2}\text{erfc}(\sqrt{\gamma_k}) = \frac{1}{2}\text{erfc}\left(\sqrt{\frac{\eta P_s \tau_0}{2\tau_k\sigma^2}}|g_k||h_k|\right) \tag{6.33}$$

by using the instantaneous SNR, where $\text{erfc}(\cdot)$ is the complementary error function of the Gaussian distribution.

Assume Nakagami-m fading channels. The joint probability density function (PDF) of $|g_k|$ and $|h_k|$ is given by Simon and Alouini (2005)

$$f_{|g_k|,|h_k|}(x_1,x_2) = \frac{4m^{m+1}(x_1x_2)^m e^{-\frac{m}{1-\rho_k}\left(\frac{x_1^2}{\Omega_1}+\frac{x_2^2}{\Omega_2}\right)}}{\Gamma(m)\Omega_1\Omega_2(1-\rho_k)(\Omega_1\Omega_2\rho_k)^{\frac{m-1}{2}}} I_{m-1}\left(\frac{2m\sqrt{\rho_k}x_1x_2}{\sqrt{\Omega_1\Omega_2}(1-\rho_k)}\right) \tag{6.34}$$

where $I_{m-1}(\cdot)$ is the $(m-1)$th order modified Bessel function of the first kind (Gradshteyn and Ryzhik 2000), $\Gamma(\cdot)$ is the Gamma function, m is the Nakagami- m parameter, Ω_1 is the average fading power in the uplink, Ω_2 is the average fading power in the downlink, and ρ_k is the correlation coefficient between $|g_k|$ and $|h_k|$. If the Jakes' model applies, using Simon and Alouini (2005), the correlation coefficient is determined by

$$\rho_k = J_0^2\left(2\pi f_m T\sum_{i=0}^{k-1}\tau_i\right) \tag{6.35}$$

where $J_0(\cdot)$ is the zeroth order Bessel function of the first kind and f_m is the maximum Doppler shift. The time difference between g_k and h_k in the fading process is given by $\sum_{i=0}^{k-1}\tau_i$, as the uplink data transmission from the users to the access point takes place sequentially.

On the other hand, the special case occurs when g_k and h_k are independent, which is the case often used in the literature and is an approximation to (6.34) when $f_m T$ or τ_k are large such that $\rho_k \to 0$. In this case, one has

$$f_{|g_k|,|h_k|}(x_1,x_2) = \frac{4m^{m+1}(x_1x_2)^{2m-1}}{\Gamma^2(m)(\Omega_1\Omega_2)^m} e^{-\frac{m}{\Omega_1}x_1^2-\frac{m}{\Omega_2}x_2^2}. \tag{6.36}$$

In the following, we are going to use (6.34) and (6.36) to derive the average achievable rate and the average BER of the kth device.

6.4.3.1 Average Achievable Rate

Using (6.34), the average achievable rate can be calculated as

$$\bar{R}_k = \int_0^\infty\int_0^\infty \tau_k\log_2\left(1+\frac{\eta P_s\tau_0}{2\sigma^2\tau_k}x_1^2x_2^2\right) f_{|g_k|,|h_k|}(x_1,x_2)dx_1dx_2 \tag{6.37}$$

which requires the solution to a two-dimensional integral. We perform a two-dimensional variable transformation as $x = x_1$ and $z = x_1x_2$. Then, using the Jacobian and its determinant, one has

$$\bar{R}_k = \int_0^\infty\int_0^\infty \tau_k\log_2\left(1+\frac{\eta P_s\tau_0}{2\sigma^2\tau_k}z^2\right) f_{|g_k|,|h_k|}\left(x,\frac{z}{x}\right)\frac{1}{x}dxdz \tag{6.38}$$

where the integrations over x_1 and x_2 have been transformed into the integrations over x and z.

For correlated links, using (6.34), the integral becomes

$$\bar{R}_k = \frac{4m^{m+1}\tau_k}{\Gamma(m)\Omega_1\Omega_2(1-\rho_k)(\Omega_1\Omega_2\rho_k)^{\frac{m-1}{2}}} \int_0^\infty \int_0^\infty \log_2\left(1+\frac{\eta P_s\tau_0}{2\sigma^2\tau_k}z^2\right) z^m \\ I_{m-1}\left(\frac{2m\sqrt{\rho_k}z}{\sqrt{\Omega_1\Omega_2}(1-\rho_k)}\right)\frac{1}{x}e^{-\frac{m}{1-\rho_k}\left(\frac{x^2}{\Omega_1}+\frac{z^2}{x^2\Omega_2}\right)}dxdz. \tag{6.39}$$

The integration over x can be solved by using an equation in Gradshteyn and Ryzhik (2000, eq. (3.478.4)) to give (Gao et al. 2018)

$$\bar{R}_k = \frac{4m^{m+1}\tau_k}{\Gamma(m)\Omega_1\Omega_2(1-\rho_k)(\Omega_1\Omega_2\rho_k)^{\frac{m-1}{2}}} \int_0^\infty \log_2\left(1+\frac{\eta P_s\tau_0}{2\sigma^2\tau_k}z^2\right) z^m \\ I_{m-1}\left(\frac{2m\sqrt{\rho_k}z}{\sqrt{\Omega_1\Omega_2}(1-\rho_k)}\right)K_0\left(\frac{2mz}{(1-\rho_k)\sqrt{\Omega_1\Omega_2}}\right)dz \tag{6.40}$$

where $K_0(\cdot)$ is the zeroth order modified Bessel function of the second kind (Gradshteyn and Ryzhik 2000). This integral cannot be simplified further unless approximations are applied. However, such a one-dimensional integral is very easy to calculate using standard mathematical software, such as MATLAB and MATHEMATICA. On the other hand, if one does need an approximation, one has (Gao et al. 2018)

$$\bar{R}_k = \frac{4m^{m+1}\tau_k}{\Gamma(m)\Omega_1\Omega_2(1-\rho_k)(\Omega_1\Omega_2\rho_k)^{\frac{m-1}{2}}} \sum_{i=0}^\infty \frac{\{m\sqrt{\rho_k}/[\sqrt{\Omega_1\Omega_2}(1-\rho_k)]\}^{m+2i-1}}{i!\Gamma(m+i)} \\ \int_0^\infty \log_2\left(1+\frac{\eta P_s\tau_0}{2\sigma^2\tau_k}z^2\right) z^{2m+2i-1}K_0\left[\frac{2mz}{(1-\rho_k)\sqrt{\Omega_1\Omega_2}}\right]dz \tag{6.41}$$

where the series expansion of $I_{m-1}(\cdot)$ in Gradshteyn and Ryzhik (2000, eq. (8.445)) has been used. The function of $K_0(x)$ decays very fast with x. It can be shown that the integrand in (6.41) is very small when $x > 10$. Thus, we can perform a least-squares curve-fitting on $K_0(x)$ for $0 < x < 10$, which gives us $K_0(x) \approx 2.7e^{-1.9x}$. Using this approximation in (6.41), one has (Gao et al. 2018)

$$\begin{aligned}\bar{R}_k &\approx \frac{10.8m^{m+1}\tau_k}{\Gamma(m)\Omega_1\Omega_2(1-\rho_k)(\Omega_1\Omega_2\rho_k)^{\frac{m-1}{2}}} \sum_{i=0}^\infty \frac{\{m\sqrt{\rho_k}/[\sqrt{\Omega_1\Omega_2}(1-\rho_k)]\}^{m+2i-1}}{i!\Gamma(m+i)\ln 2} \\ &\left[\frac{(1-\rho_k)\sqrt{\Omega_1\Omega_2}}{3.8m}\right]^{2m+2i} \int_0^\infty \ln\left[1+\frac{\eta P_s\tau_0}{2\sigma^2\tau_k}\frac{(1-\rho_k)^2\Omega_1\Omega_2}{3.8m^2}t^2\right] t^{2m+2i-1}e^{-t}dt \\ &= \frac{10.8m^{m+1}\tau_k}{\Gamma(m)\Omega_1\Omega_2(1-\rho_k)(\Omega_1\Omega_2\rho_k)^{\frac{m-1}{2}}} \sum_{i=0}^\infty \frac{\{m\sqrt{\rho_k}/[\sqrt{\Omega_1\Omega_2}(1-\rho_k)]\}^{m+2i-1}}{i!\Gamma(m+i)\ln 2} \\ &\left[\frac{(1-\rho_i)\sqrt{\Omega_1\Omega_2}}{3.8m}\right]^{2m+2i} F\left[\frac{\eta P_s\tau_0}{2\sigma^2\tau_k}\frac{(1-\rho_i)^2\Omega_1\Omega_2}{3.8m^2}, 2m+2i-1\right]\end{aligned} \tag{6.42}$$

where we have defined

$$F(a,n) = \int_0^\infty \ln(1+at^2)t^n e^{-t}dt \tag{6.43}$$

with n being an integer, and it can be solved iteratively using integration by parts as (Gao et al. 2018)

$$\begin{aligned} F(a,n) &= \int_0^\infty \ln(1+at^2)t^n e^{-t}dt \\ &= -\int_0^\infty \ln(1+at^2)t^n de^{-t} \\ &= n\int_0^\infty \ln(1+at^2)t^{n-1}e^{-t}dt + 2\int_0^\infty \frac{t^{n+1}}{1/a+t^2}e^{-t}dt \\ &= nF(a,n-1) + G(a,n) \end{aligned} \tag{6.44}$$

where $G(a,n) = (-1)^{\frac{n+1}{2}}(\frac{1}{\sqrt{a}})^n[ci(\frac{1}{\sqrt{a}})\sin(\frac{1}{\sqrt{a}}) - si(\frac{1}{\sqrt{a}})\cos(\frac{1}{\sqrt{a}})] + \sum_{j=1}^{\frac{n+1}{2}}(n+1-2j)!(-\frac{1}{a})^{j-1}$ for odd values of n, $G(a,n) = (-1)^{\frac{n}{2}-1}(\frac{1}{\sqrt{a}})^n[ci(\frac{1}{\sqrt{a}})\cos(\frac{1}{\sqrt{a}}) + si(\frac{1}{\sqrt{a}})\sin(\frac{1}{\sqrt{a}})] + \sum_{j=1}^{\frac{n}{2}}(n+1-2j)!(-\frac{1}{a})^{j-1}$ for even values of n, and $F(a,0) = \ln a + 2[\ln\frac{1}{\sqrt{a}} - ci(\frac{1}{\sqrt{a}})\cos(\frac{1}{\sqrt{a}}) - si(\frac{1}{\sqrt{a}})\sin(\frac{1}{\sqrt{a}})]$ by using Gradshteyn and Ryzhik (2000, eq. (4.338.1)), and $ci(\cdot)$ and $si(\cdot)$ are the cosine integral and the sine integral, respectively, using Gradshteyn and Ryzhik (2000, eq. (3.356.1) and eq. (3.356.2)).

Similarly, if the links are independent, using (6.36), one has

$$\bar{R}_k = \frac{4m^{2m}\tau_k}{\Gamma^2(m)(\Omega_1\Omega_2)^m}\int_0^\infty \log_2\left(1+\frac{\eta P_s\tau_0}{2\sigma^2\tau_k}z^2\right)z^{2m-1}K_0\left(\frac{2mz}{\sqrt{\Omega_1\Omega_2}}\right)dz. \tag{6.45}$$

Equation (6.45) can also be obtained from (6.42) by using the series expansion of the Bessel function $I_{m-1}(\cdot)$ (Gradshteyn and Ryzhik 2000, eq. (8.445)) and letting $\rho_k \to 0$ in the expanded result, assuming that the integration and the limiting operations can exchange orders. Using $K_0(x) \approx 2.7e^{-1.9x}$, a simpler approximation can also be derived as

$$\bar{R}_k \approx \frac{10.8m^{2m}\tau_k}{\Gamma^2(m)(\Omega_1\Omega_2)^m \ln 2}\left(\frac{\sqrt{\Omega_1\Omega_2}}{3.8m}\right)^{2m} F\left(\frac{\eta P_s\tau_0}{2\sigma^2\tau_k}\frac{\Omega_1\Omega_2}{3.8^2m^2}, 2m-1\right). \tag{6.46}$$

6.4.3.2 Average BER

Using (6.34), the average BER can be obtained as

$$\bar{B}_k = \frac{1}{2}\int_0^\infty\int_0^\infty \text{erfc}\left(\sqrt{\frac{\eta P_s\tau_0}{2\tau_k\sigma^2}}x_1x_2\right)f_{|g_k|,|h_k|}(x_1,x_2)dx_1dx_2. \tag{6.47}$$

By using the same method as that in the previous section, similar integral expressions for the average BER can be obtained. However, unlike the logarithm function, since the erfc function is convergent, integration by parts can be used to solve all the integrals. To do this, the average BER can be rewritten as

$$\bar{B}_i = \frac{1}{2}\int_0^\infty \text{erfc}\left(\sqrt{\frac{\eta P_s\tau_0}{2\tau_k\sigma^2}}z\right)f_{|g_k||h_k|}(z)dz \tag{6.48}$$

where $f_{|g_k||h_k|}(z)$ is the PDF of the random variable $|g_k||h_k|$. From (6.48), one has

$$\bar{B}_k = \frac{1}{2}\int_0^\infty \text{erfc}\left(\sqrt{\frac{\eta P_s\tau_0}{\tau_k\sigma^2}}z\right)dF_{|g_k||h_k|}(z) \tag{6.49}$$

where $F_{|g_k||h_k|}(z)$ is the cumulative distribution function (CDF) of $|g_k||h_k|$. Using integration by parts, one has from (6.49)

$$\bar{B_k} = \sqrt{\frac{\eta P_s \tau_0}{2\pi\sigma^2\tau_k}} \int_0^\infty e^{-\frac{\eta P_s \tau_0}{2\tau_k\sigma^2}z^2} F_{|g_k||h_k|}(z)dz. \tag{6.50}$$

Note that the logarithm function is not convergent so that the integration by parts will lead to divergence in the calculation. Thus, this method cannot be used in the calculation of the average achievable rate. Note also that the calculation of (6.50) requires the CDF of $|g_k||h_k|$, which will be derived next.

The CDF of $|g_k||h_k|$ is defined as

$$F_{|g_k||h_k|}(z) = Pr\{x_1x_2 < z, 0 < x_1 < \infty, 0 < x_2 < \infty\}. \tag{6.51}$$

Using the joint PDF in (6.34), this gives

$$\begin{aligned} F_{|g_k||h_k|}(z) = &\frac{4m^{m+1}}{\Gamma(m)\Omega_1\Omega_2(1-\rho_k)(\Omega_1\Omega_2\rho_k)^{\frac{m-1}{2}}} \int_0^\infty x_2^m e^{-\frac{m}{1-\rho_k}\frac{x_2^2}{\Omega_2}} \\ &\times \int_0^{z/x_2} x_1^m e^{-\frac{m}{1-\rho_k}\frac{x_1^2}{\Omega_1}} I_{m-1}\left(\frac{2m\sqrt{\rho_k}x_1x_2}{\sqrt{\Omega_1\Omega_2}(1-\rho_k)}\right)dx_1dx_2. \end{aligned} \tag{6.52}$$

Using Gradshteyn and Ryzhik (2000, eq. (8.445)), one further has (Gao et al. 2018)

$$\begin{aligned} F_{|g_k||h_k|}(z) = &\frac{4m^{m+1}}{\Gamma(m)\Omega_1\Omega_2(1-\rho_k)(\Omega_1\Omega_2\rho_k)^{\frac{m-1}{2}}} \sum_{i=0}^\infty \frac{\left[\frac{m\sqrt{\rho_k}}{\sqrt{\Omega_1\Omega_2}(1-\rho_k)}\right]^{m-1+2i}}{i!\Gamma(m+i)} \\ &\times \int_0^\infty x_2^{2m-1+2i} e^{-\frac{m}{1-\rho_k}\frac{x_2^2}{\Omega_2}} \int_0^{z/x_2} x_1^{2m+2i-1} e^{-\frac{m}{1-\rho_k}\frac{x_1^2}{\Omega_1}} dx_1dx_2. \end{aligned} \tag{6.53}$$

We solve the inner integral first, which is a function of x_2. By letting $t = x_1^2$ and using Gradshteyn and Ryzhik (2000, eq. (3.351.1)), one has

$$\begin{aligned} &\int_0^{z/x_2} x_1^{2m+2i-1} e^{-\frac{m}{1-\rho_k}\frac{x_1^2}{\Omega_1}} dx_1 \\ &= \frac{(m+i-1)!}{2(\frac{m}{(1-\rho_k)\Omega_1})^{m+i}} \left[1 - e^{-\frac{m}{1-\rho_k}\frac{z^2}{\Omega_1x_2^2}} \sum_{j=0}^{m+i-1} \frac{(z^2/x_2^2)^j}{j!}\left[\frac{(1-\rho_k)\Omega_1}{m}\right]^j\right]. \end{aligned} \tag{6.54}$$

Using (6.54) in (6.53), the integral becomes (Gao et al. 2018)

$$\begin{aligned} F_{|g_k||h_k|}(z) = &\frac{4m^{m+1}}{\Gamma(m)\Omega_1\Omega_2(1-\rho_k)(\Omega_1\Omega_2\rho_k)^{\frac{m-1}{2}}} \sum_{i=0}^\infty \frac{\left[\frac{m\sqrt{\rho_k}}{\sqrt{\Omega_1\Omega_2}(1-\rho_k)}\right]^{m-1+2i}}{2i!\left[\frac{m}{(1-\rho_k)\Omega_1}\right]^{m+i}} \\ &\times\Bigg\{ \int_0^\infty x_2^{2m-1+2i} e^{-\frac{m}{1-\rho_k}\frac{x_2^2}{\Omega_2}} dx_2 - \sum_{j=0}^{m+i-1} \frac{z^{2j}\left[\frac{(1-\rho_k)\Omega_1}{m}\right]^j}{j!} \\ &\times \int_0^\infty x_2^{2m+2i-2j-1} e^{-\frac{m}{1-\rho_k}\frac{x_2^2}{\Omega_2} - -\frac{m}{1-\rho_k}\frac{z^2}{\Omega_1x_2^2}} dx_2 \Bigg\}. \end{aligned} \tag{6.55}$$

Using equations from Gradshteyn and Ryzhik (2000, eq. (3.461.3) and eq. (3.478.4)) in (6.55), the CDF is (Gao et al. 2018)

$$F_{|g_k||h_k|}(z) = \sum_{i=0}^{\infty} \frac{2\rho_k^i m^{2m+2i}}{i!\Gamma(m)(\Omega_1\Omega_2)^{m+i}(1-\rho_k)^{m+2i}} \times \left\{ \frac{(m+i-1)!(\Omega_1\Omega_2)^{m+i}(1-\rho_i)^{2m+2i}}{2m^{2m+2i}} - \sum_{j=0}^{m+i-1} \frac{1}{j!}\left[\frac{z(1-\rho_k)\sqrt{\Omega_1\Omega_2}}{m}\right]^{m+j-i} K_{m+j-i}\left[\frac{2mz}{(1-\rho_k)\sqrt{\Omega_1\Omega_2}}\right] \right\}. \quad (6.56)$$

Then, the average BER can be derived by substituting (6.56) into (6.50), which gives

$$\begin{aligned}\bar{B}_k = &\sqrt{\frac{\eta P_s \tau_0}{2\pi\sigma^2\tau_k}} \sum_{i=0}^{\infty} \frac{2\rho_k^i m^{2m+2i}}{i!\Gamma(m)(\Omega_1\Omega_2)^{m+i}(1-\rho_k)^{m+2i}} \\ &\left\{ \frac{(m+i-1)!(\Omega_1\Omega_2)^{m+i}(1-\rho_k)^{2m+2i}}{2m^{2m+2i}} \right. \\ &\times \int_0^{\infty} e^{-\frac{\eta P_s \tau_0}{2\tau_k\sigma^2} z^2} dz - \sum_{j=0}^{m+i-1} \frac{1}{j!}\left[\frac{(1-\rho_k)\sqrt{\Omega_1\Omega_2}}{m}\right]^{m+j-i} \\ &\left. \times \int_0^{\infty} z^{m+i+j} e^{-\frac{\eta P_s \tau_0}{2\tau_k\sigma^2} z^2} K_{m+j-i}\left[\frac{2mz}{(1-\rho_k)\sqrt{\Omega_1\Omega_2}}\right] dz \right\}. \end{aligned} \quad (6.57)$$

Solving the two one-dimensional integrals using equations in Gradshteyn and Ryzhik (2000, eq. (3.461.3) and eq. (6.631.3)), one can derive the average BER as (Gao et al. 2018)

$$\begin{aligned}\bar{B}_k = &\sqrt{\frac{\eta P_s \tau_0}{2\pi\sigma^2\tau_k}} \sum_{i=0}^{\infty} \frac{2\rho_k^i m^{2m+2i}}{i!\Gamma(m)(\Omega_1\Omega_2)^{m+i}(1-\rho_k)^{m+2i}} \\ &\times \left\{ \frac{(m+i-1)!(\Omega_1\Omega_2)^{m+i}(1-\rho_k)^{2m+2i}}{4m^{2m+2i}\sqrt{\eta P_s \tau_0/(2\pi\tau_k\sigma^2)}} \right. \\ &- \sum_{j=0}^{m+i-1} \frac{1}{j!}\left[\frac{(1-\rho_k)\sqrt{\Omega_1\Omega_2}}{m}\right]^{m+i-j+1} \frac{\Gamma(m+i+0.5)\Gamma(j+0.5)}{4\left(\sqrt{\frac{\eta P_s \tau_0}{2\tau_k\sigma^2}}\right)^{m+j+i}} \\ &\left. \times e^{\frac{m^2\tau_k\sigma^2}{2(1-\rho_k)^2\Omega_1\Omega_2\eta P_s\tau_0}} W_{-\frac{m+j+i}{2},\frac{m+j-i}{2}}\left[\frac{2m^2\tau_k\sigma^2}{(1-\rho_k)^2\Omega_1\Omega_2\eta P_s\tau_0}\right] \right\} \end{aligned} \quad (6.58)$$

where $W(\cdot)$ is the Whittaker function (Gradshteyn and Ryzhik 2000).

When the links are independent, using a similar method, the average BER in this case is given by

$$\begin{aligned}\bar{B}_k = &\frac{1}{2} - \frac{1}{2}\frac{m^{m-1}}{\Gamma(m)\sqrt{\pi}(\Omega_1\Omega_2)^{\frac{m-1}{2}}}\left(\sqrt{\frac{\eta P_s\tau_0}{2\tau_i\sigma^2}}\right)^{1-m} \sum_{i=0}^{m-1} \frac{\Gamma(m+0.5)\Gamma(i+0.5)}{i!} \\ &\times\left(m\sqrt{\frac{2\tau_k\sigma^2}{\Omega_1\Omega_2\eta P_s\tau_0}}\right)^{i} e^{\frac{m^2\tau_k\sigma^2}{2\eta P_s\tau_0\Omega_1\Omega_2}} W_{-\frac{m+i}{2},\frac{m-i}{2}}\left(\frac{2m^2\tau_k\sigma^2}{\eta P_s\tau_0\Omega_1\Omega_2}\right). \end{aligned} \quad (6.59)$$

One can also let $m = 1$ to obtain the results for Rayleigh fading channels. This will simplify the results further.

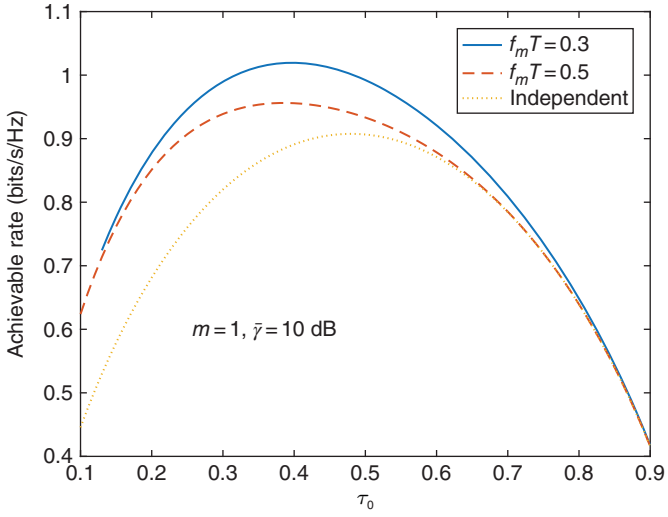

Figure 6.10 Average rate versus τ_0 for different values of f_mT in the Jakes' model.

6.4.3.3 Numerical Examples

In this section, the performance of wireless powered communications (WPC) will be examined through numerical examples using the average rate and the average BER. In the examination, we set $\eta = 0.5$, and $\Omega_1 = \Omega_2 = 1$, while we vary the values of τ_0,f_mT, m, and $\bar{\gamma} = \frac{P_s}{2\sigma^2}$. For simplicity, we only consider the case of one user such that $\tau_0 + \tau_1 = 1$, except in Figure 6.20.

Figures 6.10–6.16 examine the average rate performance of the WPC system under different conditions. In particular, Figure 6.10 shows the achievable rate versus τ_0 for different values of f_mT. The value of f_mT determines the correlation of the links. The smaller the value of f_mT is, the more correlated the links will be. Several observations can be made from Figure 6.10. First, there exists an optimum τ_0 in all the cases considered, as expected, as a larger τ_0 generates more harvested power and higher SNR in the received signal at the access point, but it also reduces the effective time for data transmission. Secondly, different values of f_mT give different achievable rates. For example, the optimum τ_0 for $f_mT = 0.5$ is around 0.4, while the optimum τ_0 for independent links is around 0.5. Their maximum achievable rates are different too. Thus, the link correlation does affect the system performance. On the other hand, when $\tau_0 > 0.6$, their performances are very similar. From (6.35), $\rho_1 = J_0^2(2\pi f_mT\tau_0)$. Thus, the correlation coefficient in general decreases when τ_0 increases. When $\tau_0 = 0.6$ and $f_mT = 0.5$, one can find that $\rho_1 \approx 0.08$, which is very close to 0. Thus, although the correlation affects the performance, this effect may be ignored when the correlation coefficient is small. Finally, if one considers the independent links as the case when $f_mT \to \infty$, one sees that the achievable rate increases and the optimum τ_0 decreases when f_mT decreases, as the link correlation benefits the performance and for smaller correlation a larger value of τ_0 is needed to harvest more power.

Figures 6.11 and 6.12 show the average rate versus τ_0 for different values of $\bar{\gamma}$ and m, respectively. One sees that the achievable rate performance of the WPC system can be significantly affected by the values of $\bar{\gamma}$ and m. Specifically, the achievable rate increases

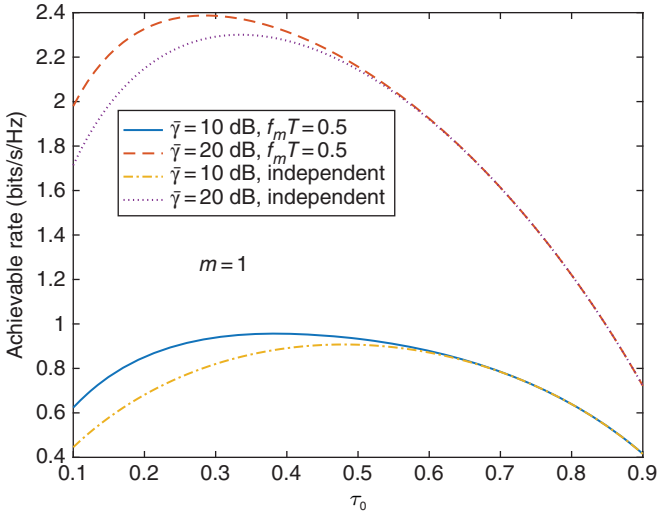

Figure 6.11 Average rate versus τ_0 for different values of $\bar{\gamma}$ in the channel.

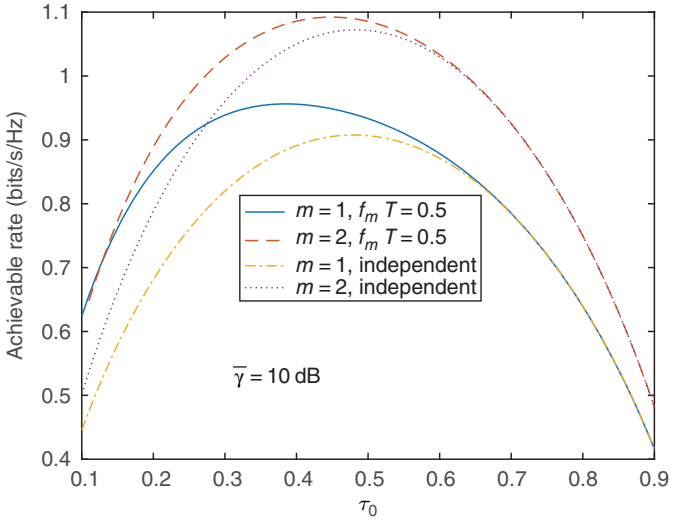

Figure 6.12 Average rate versus τ_0 for different values of the Nakagami-*m* parameter in the channel.

when $\bar{\gamma}$ and m increase, as expected, as the channel conditions become better for larger values of $\bar{\gamma}$ and m. In Figure 6.11, the optimum τ_0 decreases when $\bar{\gamma}$ increases, while in Figure 6.12, the optimum τ_0 increases when m increases. Similar to Figure 6.10, comparing the performance for correlated links with that for independent links, one sees that their performances are similar when τ_0 is large due to low correlation but are significantly different when τ_0 is small with large correlation.

Figures 6.13 and 6.14 show the maximum achievable rate and the optimum τ_0 versus $\bar{\gamma}$ for different values of $f_m T$, respectively. One sees from Figure 6.13 that the difference caused by link correlation increases when $\bar{\gamma}$ increases or $f_m T$ decreases, as expected. For

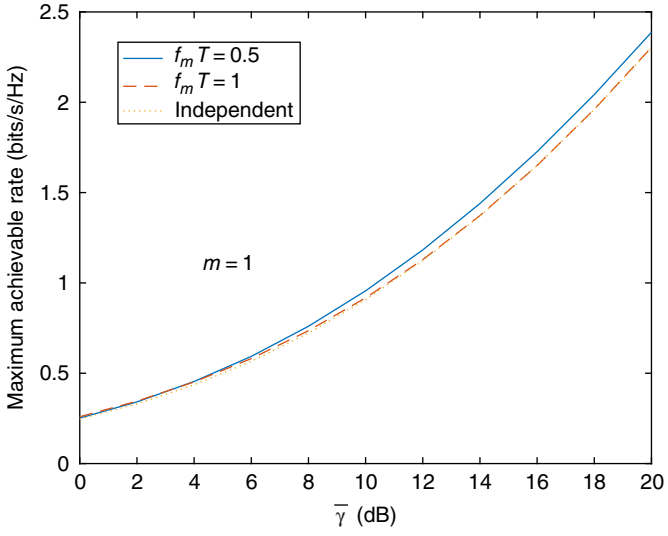

Figure 6.13 Maximum average rate versus $\bar{\gamma}$ for different values of $f_m T$ in the Jakes' model.

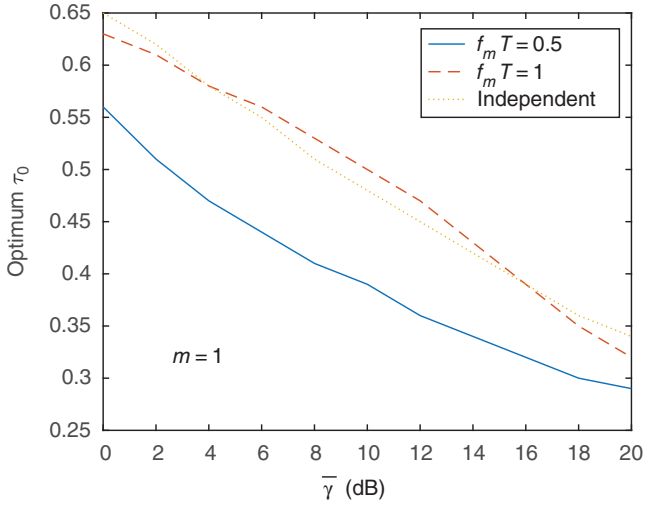

Figure 6.14 Optimum τ_0 versus $\bar{\gamma}$ for different values of $f_m T$ in the Jakes' model.

small $\bar{\gamma}$ and large $f_m T$, the difference is negligible. On the other hand, from Figure 6.14, the optimum values of τ_0 that reach the maximum achievable rates are significantly different between correlated links and independent links. For example, when $\bar{\gamma} = 10$ dB, the optimum τ_0 for independent links is 0.5, while the optimum τ_0 for correlated links is around 0.38. Since the maximum value of τ_0 is 1, this represents a 12% difference.

Figures 6.15 and 6.16 show the maximum achievable rate and the optimum τ_0 versus $\bar{\gamma}$ for different values of m, respectively. From Figure 6.15, the maximum achievable rate increases when m increases. However, the difference between correlated links and

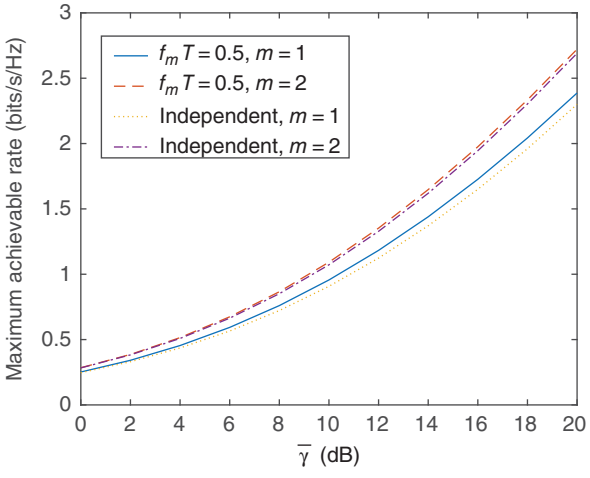

Figure 6.15 Maximum average rate versus $\bar{\gamma}$ for different values of the Nakagami-m parameter in the channel.

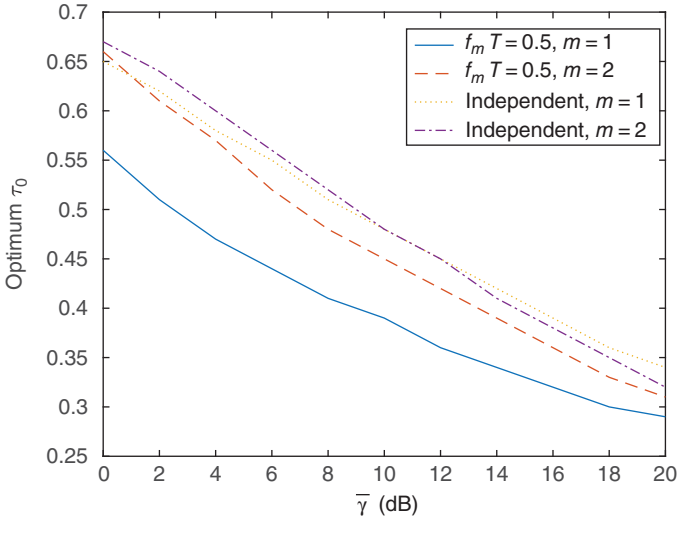

Figure 6.16 Optimum τ_0 versus $\bar{\gamma}$ for different values of the Nakagami-m parameter in the channel.

independent links decreases when m increases. This implies that the link correlation is not important when the channel condition is good enough, as it can compensate the performance degradation caused by low link correlation. Similarly, from Figure 6.16, the optimum τ_0 increases when m increases but the difference between correlated links and independent links also decreases when m increases. For example, when $\bar{\gamma} = 10$ dB, $m = 1$ gives the optimum τ_0 of 0.38 for $f_m T = 0.5$ and the optimum τ_0 of 0.5 for independent links, while $m = 2$ gives the optimum τ_0 of 0.45 for $f_m T = 0.5$ and the optimum τ_0 of 0.5 for independent links.

Figures 6.17–6.19 show the average BER performance of the system for different parameters. One sees from these figures that the BER decreases when $\bar{\gamma}$ increases or m increases. However, the BER changes little when $f_m T$ changes in the cases considered,

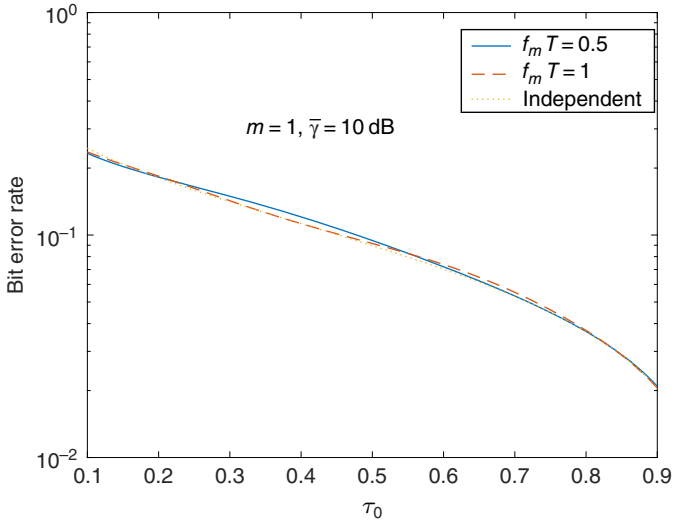

Figure 6.17 Average BER versus τ_0 for different values of $f_m T$ in the Jakes' model.

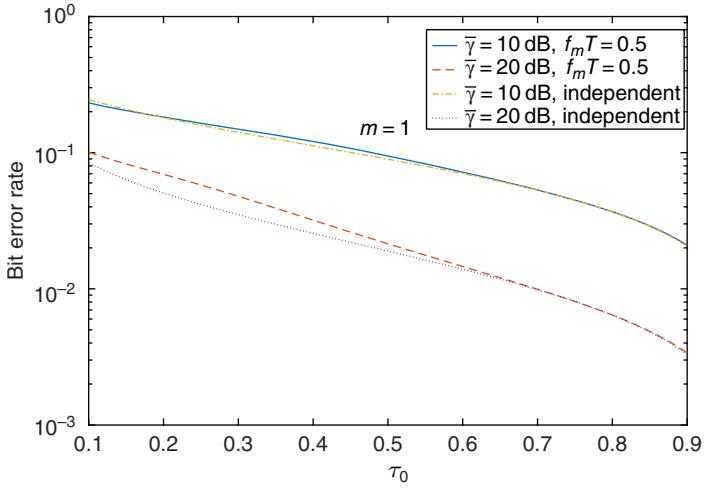

Figure 6.18 Average BER versus τ_0 for different values of $\bar{\gamma}$ in the channel.

implying that the link correlation does not affect the BER performance of the system much. Also, the BER always decreases when τ_0 increases, as a larger τ_0 will produce more harvested power and hence higher SNR in the received signal.

Figure 6.20 shows the average sum rate of two users versus τ_0, when $\bar{\gamma} = 10$ dB, $f_m T = 0.5$, and $m = 1$ for different values of τ_1. In this case, $\tau_0 + \tau_1 + \tau_2 = 1$. One sees that there exists an optimum τ_0 that maximizes the average sum rate for a fixed value of τ_1. When the value of τ_1 increases from 0.05 to 0.30 with a step size of 0.05, the maximum rate increases and the corresponding optimum τ_0 decreases. When τ_1 is

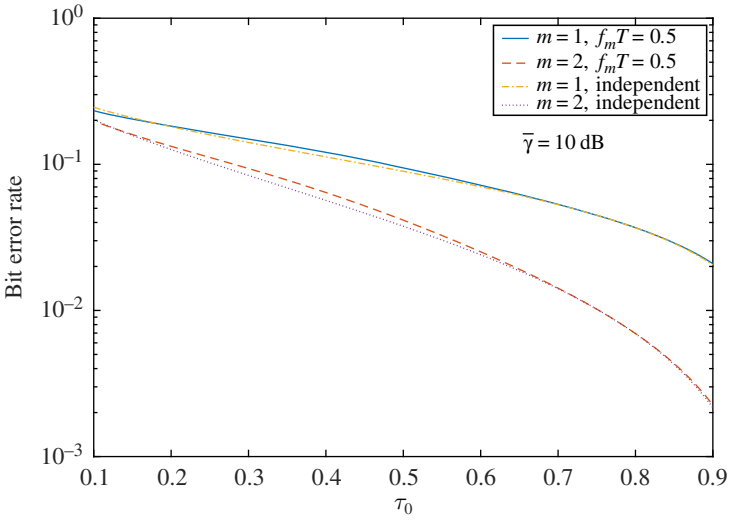

Figure 6.19 Average BER versus τ_0 for different values of the Nakagami-*m* parameter in the channel.

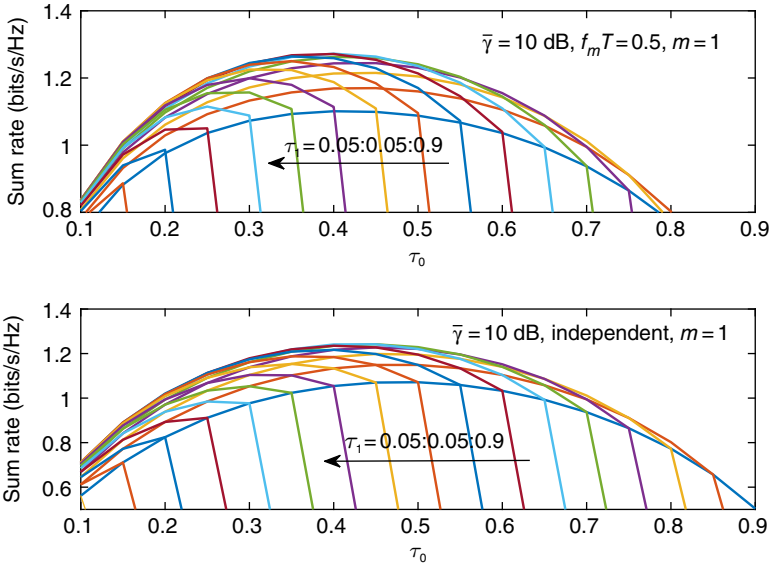

Figure 6.20 Average sum rate versus τ_0 for two devices.

larger than 0.30 and keeps increasing, the maximum rate decreases again, implying that there is a global maximum sum rate.

In summary, the tradeoff between energy and information for the HAP wireless powered communications is considered for the use of the same link. The balance between the power transfer time and the information delivery time needs to be studied. This leads to many optimization problems, including the basic ones discussed in this section. More details on the derivation can be found in Gao et al. (2018).

6.5 Power Beacon

PB is the last form of wireless powered communications that will be discussed here. Compared with SWIPT and HAP, in PB-based wireless powered communications, wireless power transfer and wireless information transmission are more independent of each other. For SWIPT, the same RF signal has to be used to deliver both power and information. For HAP, the same link has to be shared in a TDD manner for power and information. However, for PB, a separate power network composed of multiple PBs is implemented to deliver power. To avoid interfering with the base station that delivers information, PB often operates at a different frequency band. Also, at the remote nodes, two sets of antennas and RF fronts are required, one for information and one for power. Thus, PB-based wireless powered communications simplifies the tradeoff between energy and information, at the cost of additional infrastructure.

Since power transfer and information delivery are relatively independent of each other in PB, not much research work needs to be done in terms of their tradeoff. Compared with conventional wireless communications systems, the only change here is that the power is delivered by RF signals instead of battery. Thus, most research on PB focuses on how the RF power can be delivered efficiently and on time, for example, by using full-duplex radios (Chalise et al. 2017), by designing waveforms for power transfer (Ku et al. 2016), and by combining it with HAP or SWIPT (Ma et al. 2015).

The only resource that has to be shared by both energy and information in PB is perhaps the space, as the power network overlays with the information network. Hence, the spatial distribution of PBs and base stations need to be coordinated. Another constraint is the energy causality, as energy has to be harvested before it can be used. These aspects are discussed in the following sections.

6.5.1 System and Design Problem

Consider a hybrid communications–power network where multiple base stations, multiple PBs, and multiple mobile nodes are randomly distributed with densities of λ_b, λ_p, and λ_m, respectively, in a certain area. The transmission power of the mobile is p, and the transmission power of the PB is q. Figure 6.21 shows the structure of a mobile receiver that can be used in such a PB-based wireless powered communications system. Since the energy storage unit cannot charge and supply power at the same time, two energy storage units are needed, one for charging and one for power supply for the data transmission. Their roles will be switched, depending on the status of the power receiver and the data transceiver.

There are two performance metrics. The first one is the signal outage at the base station that serves a specific mobile. It can be given as

$$P_O = Pr\left\{\frac{p/d_1^{\alpha}}{I+\sigma^2} < \gamma_0\right\} \tag{6.60}$$

where d_1 is the random distance between the base station and the mobile, α is the path loss exponent, $I+\sigma^2$ is the interference-plus-noise power, and γ_0 is the threshold. Thus, if the signal from the mobile to the base station has a signal-to-interference-plus-noise ratio (SINR) below a threshold, the base station will not be able to detect this signal and hence a signal outage occurs. The second one is the power outage at the mobile. If

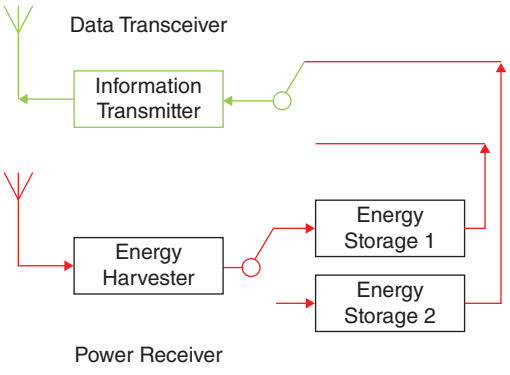

Figure 6.21 A mobile receiver used in PB-based wireless powered communications.

the mobile has a limited storage and the instantaneous power it receives from the PB is not enough for the next transmission, a power outage occurs. This only happens when the energy storage is limited. If the energy storage is unlimited, the power outage may not occur.

The power transfer can be performed in two ways: isotropic power transfer; or directed power transfer. Isotropic transfer uses an omnidirectional antenna, while directed transfer uses a directional antenna or array. In the case of isotropic transfer, the mobile receives power from all PBs within the range so that the received instantaneous power is

$$P = \sum_{i \in \Phi} \frac{qd}{[\max\{d_i, v\}]^{\beta}} \tag{6.61}$$

where Φ represents the set of PBs within the range, d_i is the distance between the mobile and the ith PB in Φ, $v \geq 1$ is a constant, d is the reference path loss, and β is the path loss exponent between mobiles and PBs. Here, the non-singular path loss model is used to avoid the issue in the traditional Friis formula that the path loss decreases when the distance increases for distances smaller than 1 m. In the case of directed transfer, the mobile will receive power from the mainlobe of the nearest PB serving it as well as sidelobes from other PBs. The received instantaneous power is

$$P = \frac{c_m qd}{[\max\{d_2, v\}]^{\beta}} + \sum_{j \in \Psi} \frac{c_s qd}{[\max\{d_j, v\}]^{\beta}} \tag{6.62}$$

where c_m is a constant representing the mainlobe response, d_2 is the distance between the mobile and its nearest PB, Ψ is the set of all PBs that affect the mobile, $c_s < c_m$ is the sidelobe response of all other PBs, d_j is the distance between the mobile and the jth PB in Ψ, and all other symbols are defined as before.

The design goals here are to find all possible combinations of p, q, λ_p, and λ_b that allow the signal outage to be smaller than a threshold ϵ and the power outage to be smaller than a threshold δ. These parameters are all larger than 0. It has been derived in Huang and Lau (2014) that, for isotropic transfer, these system parameters must satisfy (Huang and Lau 2014)

$$q\lambda_p \lambda_b^{\frac{\alpha}{2}} \geq (1 - \frac{2}{\beta}) \frac{\omega \sigma^2 v^{\beta-2}}{\pi e d \mu} \tag{6.63}$$

where ω is the duty cycle scheduled by the base station for the mobile to transmit information, σ^2 is the noise power at the base station, e and d are the reference path losses in the communications network and the power network, respectively, and μ is a constant determined by ϵ. A curve between μ and ϵ has been provided in Huang and Lau (2014).

For directed transfer, they also satisfy (Huang and Lau 2014)

$$c_m q \lambda_b^{\frac{\alpha}{2}} (1 - e^{-\pi \lambda_p v^2}) \geq \frac{\omega \sigma^2 v^\beta}{ed\mu} \tag{6.64}$$

which is a subset of (6.42). Equations (6.42) and (6.43) are for unlimited energy storage at the mobile.

In the case when the energy storage is limited, for isotropic transfer, one has (Huang and Lau 2014)

$$q \lambda_p^{\frac{\beta}{2}} \lambda_b^{\frac{\alpha}{2}} \geq \left(\frac{-\log \delta}{\pi} \right)^{\frac{\beta}{2}} \frac{\sigma^2}{ed\mu} \tag{6.65a}$$

$$q \lambda_b^{\frac{\alpha}{2}} \geq \frac{\sigma^2 v^\beta}{ed\mu} \tag{6.65b}$$

and for directed transfer, one has (Huang and Lau 2014)

$$z_m q \lambda_p^{\frac{\beta}{2}} \lambda_b^{\frac{\alpha}{2}} \geq \left(\frac{-\log \delta}{\pi} \right)^{\frac{\beta}{2}} \frac{\sigma^2}{ed\mu} \tag{6.66a}$$

$$z_m q \lambda_b^{\frac{\alpha}{2}} \geq \frac{\sigma^2 v^\beta}{ed\mu}. \tag{6.66b}$$

A detailed discussion of these equations can be found in Huang and Lau (2014). Note that all these results are based on stochastic geometry models with randomly distributed base stations, PBs and mobiles. There has been no system level simulation of these results. The actual implementation is likely to be more complicated; especially the coordination between the wireless power network and the wireless communications network requires considerable effort.

6.5.2 More Notes

In summary, PB-based wireless powered communications require more infrastructure support in terms of extra PBs and extra RF fronts than SWIPT and HAP, but with a simpler tradeoff between energy and information. Thus, most research in PB-based wireless powered communications focuses on the RF power transfer and the PB network deployment, as the communications side of this system has been well studied. For SWIPT and HAP, power transfer and information delivery have to share the same signal or the same link. Hence, the tradeoff in these wireless powered communications is more complicated, and most of the research focuses on this tradeoff in different applications, such as multi-input-multiple-output (Zhang and Ho 2013), physical layer security (Liu et al. 2014a), joint time and power allocation (Luo et al. 2013), and even joint resource allocation and power splitting (Shi et al. 2014). A common point is that all these works study the fundamental tradeoff between energy and information. In the following, some of these interesting studies will be discussed. To have a complete view of all these studies, a cited reference search of Grover and Sahai (2010), Zhou et al. (2013b), or Ju and Zhang (2014) will be helpful.

6.6 Other Issues

6.6.1 Effect of Interference on Wireless Power

The interference in a wireless network normally degrades the system performance, as it reduces the SINR. There have been quite a few studies on the effect of interference on wireless powered communications. For example, Diamantoulakis et al. (2017) examined the effect of interference on HAP. Zhong et al. (2015a) studied the effect of interference on the throughput of a PB scheme. In Liu et al. (2013), the effect of interference on the scheduling of energy and information at the transmitter was studied. In Shen et al. (2014), a multi-user interference channel was considered by maximizing the sum rate subject to energy harvesting constraints. In Chen et al. (2017a), the effect of interference generated by sending wireless power was studied.

On the other hand, interference is also a good source of energy. In particular, for wireless powered communications, interference is some ambient RF energy that can actually be harvested for power. Consequently, this may improve the data transmission later due to a higher transmission power. In Zhao et al. (2017b), a detailed survey on the use of interference in energy harvesting has been provided.

Thus, it is interesting to study these two contradicting effects of interference on wireless powered systems. In the following, the HAP system is considered. In this system, the interference can increase the amount of the power received at the nodes in the downlink. This increased power could be used to send the information back to the HAP using a higher transmission power, to compensate the reduced SINR due to interference in the uplink. Rayleigh fading channels are used. The average SINR and the average rate will be derived next.

6.6.1.1 System and Assumptions

As discussed before, in HAP, power transfer and information transmission are performed sequentially. The base station first transmits energy to the nodes for τ_0 seconds. The nodes harvest this energy and uses it to transmit data to the base station for τ_1 seconds, where $\tau_0 + \tau_1 = T$ is the total time.

Using this assumption, the signal received by the node in the downlink is

$$y = \sqrt{P_s}h + \sum_{i=1}^{N} \sqrt{Q_i}u_i x_i + n \tag{6.67}$$

where P_s is the transmission power of the base station, h is the fading channel gain and is a complex Gaussian random variable with mean zero and variance $2\alpha_h^2$, N is the number of interferes in the downlink, Q_i is the transmission power of the ith interferer, u_i is the fading gain from the ith interferer and is a complex Gaussian random variable with mean zero and variance $2\alpha_{u_i}^2$, x_i is the transmitted symbol of the ith interferer with $E\{|x_i|^2\} = 1$, $E\{\cdot\}$ is the expectation operator, and n is the AWGN with mean zero and variance $2\sigma^2$. This signal is harvested, and the harvested energy is given by

$$E_h = \eta(P_s|h|^2 + \sum_{i=1}^{N} Q_i|u_i|^2)\tau_0 \tag{6.68}$$

where η is the conversion efficiency of the energy harvester. From this equation, the interference increases the amount of energy harvested.

The harvested energy is then used to transmit the information to the base station. The signal received by the base station is

$$z = \sqrt{P_r} g x + \sum_{j=1}^{M} \sqrt{T_j} v_j x_j + n \tag{6.69}$$

where $P_r = \frac{\tau_0}{\tau_1}\eta(P_s|h|^2 + \sum_{i=1}^{N} Q_i|u_i|^2)$ is the node transmission power using the harvested energy, g is the complex Gaussian fading gain with mean zero and variance $2\alpha_g^2$, x is the transmitted signal with $E\{|x|^2\} = 1$, M is the number of interfering nodes, T_j is the jth interfering node's transmission power, v_j is the fading gain from the jth interfering node and is a complex Gaussian random variable with mean zero and variance $2\alpha_{v_j}^2$, x_j is the transmitted symbol with $E\{|x_j|^2\} = 1$, and n is again the noise with mean zero and variance $2\sigma^2$. Thus, the SINR in this case is

$$\gamma = \frac{\tau_0}{\tau_1}\eta|g|^2 \frac{P_s|h|^2 + \sum_{i=1}^{N} Q_i|u_i|^2}{\sum_{j=1}^{M} T_j|v_j|^2 + 2\sigma^2}. \tag{6.70}$$

It can be seen that the interference increases the SINR in the numerator while decreasing the SINR in the denominator. The actual effect of the interference cannot be observed from this equation, and has to be analyzed.

6.6.1.2 Performances with Interference

First, the probability density functions (PDFs) of two random variables are needed. In the numerator, let $S = P_s|h|^2 + \sum_{i=1}^{N} Q_i|u_i|^2$. Since $|h|^2, |u_i|^2, i = 1, 2, \cdots, N$ are independent exponential random variables, one has (Johnson et al. 1994)

$$f_S(s) = \sum_{i=0}^{N} \frac{\prod_{k=0}^{N} \frac{1}{2\alpha_{u_k}^2 Q_k}}{\prod_{k=0,k\neq i}^{N} (\frac{1}{2\alpha_{u_k}^2 Q_k} - \frac{1}{2\alpha_{u_i}^2 Q_i})} e^{-\frac{s}{2\alpha_{u_i}^2 Q_i}}, \; s > 0 \tag{6.71}$$

where $\alpha_{u_0} = \alpha_h$ and $Q_0 = P_s$. In the denominator, defining $\Omega = \sum_{j=1}^{M} T_j|v_j|^2$, one has

$$f_\Omega(w) = \sum_{j=1}^{M} \frac{\prod_{k=1}^{M} \frac{1}{2\alpha_{v_k}^2 T_k}}{\prod_{k=1,k\neq j}^{M} (\frac{1}{2\alpha_{v_k}^2 T_k} - \frac{1}{2\alpha_{v_j}^2 T_j})} e^{-\frac{w}{2\alpha_{v_j}^2 T_j}}, \; w > 0. \tag{6.72}$$

The average SINR of the signal received by the base station is obtained as

$$\bar{\gamma} = \frac{\tau_0}{\tau_1}\eta 2\alpha_g^2 (2\alpha_h^2 P_s + \sum_{i=1}^{N} 2\alpha_{u_i}^2 Q_i) E\left\{\frac{1}{\Omega + 2\sigma^2}\right\} \tag{6.73}$$

where

$$E\left\{\frac{1}{\Omega + 2\sigma^2}\right\} = -\sum_{j=1}^{M} \frac{\prod_{k=1}^{M} \frac{1}{2\alpha_{v_k}^2 T_k} e^{\frac{\sigma^2}{\alpha_{v_j}^2 T_j}} Ei(-\frac{\sigma^2}{\alpha_{v_j}^2 T_j})}{\prod_{k=1,k\neq j}^{M} (\frac{1}{2\alpha_{v_k}^2 T_k} - \frac{1}{2\alpha_{v_j}^2 T_j})} \tag{6.74}$$

using an equation in Gradshteyn and Ryzhik (2000, eq. (3.352.4)), and $Ei(\cdot)$ is the exponential integral (Gradshteyn and Ryzhik 2000, eq. (8.211.1)).

The average rate is derived as

$$\bar{\tau} = E\{\tau_1 \log_2(1+\gamma)\} = I_1 - I_2 \tag{6.75}$$

where, using an equation in Gradshteyn and Ryzhik (2000, eq. (4.337.1)), one has

$$I_1 = \sum_{j=1}^{M} \frac{\tau_1 \prod_{k=1}^{M} \frac{1}{2\alpha_{v_k}^2 Q_k} 2\alpha_{v_j}^2 Q_j}{\ln 2 \prod_{k=1,k\neq j}^{M} \left(\frac{1}{2\alpha_{v_k}^2 Q_k} - \frac{1}{2\alpha_{v_j}^2 Q_j}\right)} \int_0^{\infty} f_Z(z) \times \left[\ln\left(2\sigma^2 + \frac{c\eta z}{1-c}\right) - e^{\frac{2\sigma^2 + \frac{\tau_0 \eta z}{\tau_1}}{2\alpha_{v_j}^2 Q_j}} Ei\left(-\frac{2\sigma^2 + \frac{c\eta z}{1-c}}{2\alpha_{v_j}^2 Q_j}\right)\right] dz. \tag{6.76}$$

and

$$I_2 = \frac{\tau_1}{\ln 2} \sum_{j=1}^{M} \frac{\prod_{k=1}^{M} \frac{1}{2\alpha_{v_k}^2 Q_k} 2\alpha_{v_j}^2 Q_j}{\prod_{k=1,k\neq j}^{M} \left(\frac{1}{2\alpha_{v_k}^2 Q_k} - \frac{1}{2\alpha_{v_j}^2 Q_j}\right)} \times \left[\ln(2\sigma^2) - e^{\frac{\sigma^2}{\alpha_{v_j}^2 Q_j}} Ei\left(-\frac{\sigma^2}{\alpha_{v_j}^2 Q_j}\right)\right]. \tag{6.77}$$

with $f_Z(z) = \frac{1}{\alpha_g^2} \sum_{i=0}^{N} \frac{\prod_{k=0}^{N} \frac{1}{2\alpha_{u_k}^2 W_k} K_0\left(2\sqrt{\frac{z}{2\alpha_{u_i}^2 W_i 2\alpha_g^2}}\right)}{\prod_{k=0,k\neq i}^{N} \left(\frac{1}{2\alpha_{u_k}^2 W_k} - \frac{1}{2\alpha_{u_i}^2 W_i}\right)}$, by using $Z = |g|^2 S$ and an equation in Gradshteyn and Ryzhik (2000, eq. (3.471.9)), $K_0(\cdot)$ is the zeroth order modified Bessel function of the second type (Gradshteyn and Ryzhik Gradshteyn and Ryzhik, (8.407.1)).

6.6.1.3 Performances without Interference

For comparison, the case of no interference is also discussed below. In this case, the two interference terms in (6.70) can be removed. Thus, the SINR becomes

$$\gamma = \frac{\tau_0}{\tau_1} \eta |g|^2 \frac{P_s |h|^2}{2\sigma^2}. \tag{6.78}$$

Then, it is quite straightforward to derive the average SINR as

$$\bar{\gamma} = \frac{2\tau_0}{\tau_1} \eta \alpha_g^2 \alpha_h^2 \frac{P_s}{\sigma^2}. \tag{6.79}$$

The average rate is derived as

$$\bar{\tau} = \tau_1 \int_0^{\infty} \log_2\left(1 + \frac{\tau_0}{\tau_1} \frac{\eta P_s}{2\sigma^2} y\right) f_Y(y) dy \tag{6.80}$$

where $Y = |g|^2 |h|^2$ and $f_Y(y) = \frac{1}{2\alpha_g^2 \alpha_h^2} K_0\left(2\sqrt{\frac{y}{4\alpha_g^2 \alpha_h^2}}\right)$.

6.6.1.4 Numerical Examples

Next, the performance of HAP with interference is compared with that without interference to examine the overall effect of interference. In the comparison, $\tau_0 = 0.5$, $T = 1$, $\eta = 0.5$, $\gamma_0 = 3$, $P_s = 1$, $W_i = 1$, and $Q_j = 1$. Also, let $SNRh = \frac{\alpha_h^2}{\sigma^2}$, $SIRh = \frac{\alpha_h^2}{A_u^2}$, and $EI = \frac{A_u^2}{A_v^2}$

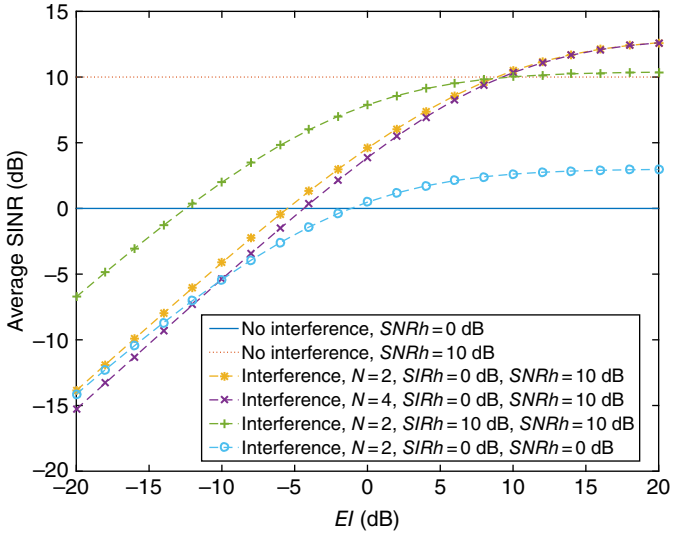

Figure 6.22 Average SINR versus *EI* for different values of *SNRh*, *SIRh* and *N*.

be the SNR of the downlink, the signal-to-interference ratio of the downlink, and the ratio of the interference power in the downlink to that in the uplink, respectively, where $A_u^2 = \sum_{i=1}^{N} \alpha_{u_i}^2 W_i$ and $A_v^2 = \sum_{j=1}^{M} \alpha_{v_j}^2 Q_j$. Also, set $M = N$, $[\alpha_{u_1}^2, \alpha_{u_2}^2, \cdots, \alpha_{u_N}^2] = [2^1, 2^2, \cdots, 2^N] \frac{A_u^2}{\sum_{i=1}^{N} 2^i}$ and $[\alpha_{v_1}^2, \alpha_{v_2}^2, \cdots, \alpha_{v_M}^2] = [2^1, 2^2, \cdots, 2^M] \frac{A_v^2}{\sum_{j=1}^{M} 2^j}$. Further, $\alpha_h^2 = \alpha_g^2 = 1$ so that A_u^2 changes with *SIRh*, A_v^2 changes with *EI*, and σ^2 changes with *SNRh*. The parameter of *EI* determines the relative strength of the interference in the downlink that contributes to energy harvesting to the strength of the interference in the uplink that reduces the SINR. It reflects the tradeoff between harm and benefit done by interference.

Figure 6.22 shows the average SINR versus *EI*. One sees that the average SINR with interference is larger than that without interference when *EI* is larger than around 9 dB when $SNRh = 10$ dB. Thus, the interference in the downlink needs to be at least 10 times as much as that in the uplink in order to make it beneficial. For $SNRh = 0$ dB, the average SINR with interference is larger than that without interference when *EI* is larger than around -1 dB. Thus, as *SNRh* decreases, it is easier to benefit from interference. Also, when *SIRh* increases or N decreases, the performance difference decreases, as expected. In this case, the threshold beyond which the average SINR with interference is larger than that without interference remains approximately the same. Finally, when *EI* increases, an upper limit occurs, as for large *EI*, the term $\sum_{j=1}^{M} \alpha_{v_j}^2 T_j$ in (6.70) can be ignored such that the performance is determined by *SNRh* and *SIRh*, which are fixed for each curve in our figures. Figure 6.23 shows the average rate versus *EI*. Similar insights can be obtained. Note that the thresholds between interference and no interference are larger than that in Figure 6.22.

In conclusion, the overall effect of interference, beneficial or harmful, is largely determined by the SNR and the ratio of the interference powers but it is always beneficial beyond a certain threshold. A more detailed discussion on this issue can be found in Chen et al. (2016a).

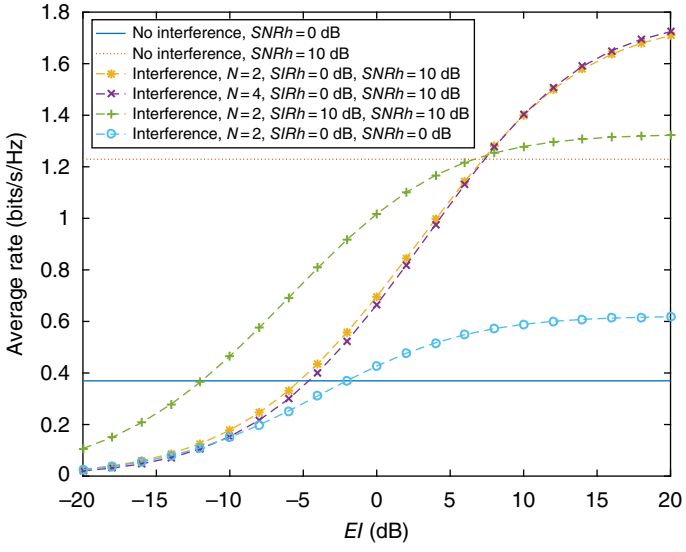

Figure 6.23 Average rate versus *EI* for different values of *SNRh*, *SIRh* and *N*.

6.6.2 Effect of Interference by Wireless Power

In the previous subsection, the effect of interference caused by information transmission on the performance of wireless powered communications has been investigated. In this subsection, we will change the angle of view by examining the effect of interference caused by wireless power on the performance of information transmission.

Interference is well known as one of the most fundamental limits in wireless networks. When wireless powered communications is performed, this issue becomes even more severe, as the use of wireless power will generate more and larger interference, which degrades the performances of information users in the same network. Effectively, due to wireless power, all the battery power and mains connection in the conventional networks become interference. For instance, in the PB networks, wireless power is broadcast by the PB to the whole network. This will introduce extra interference to all devices operating at the same frequency band, even though they may not need wireless power. In SWIPT, in order to deliver power and information by using the same signal, the transmission power needs to be raised so that there is enough energy to be split either in the time domain or the power domain at the receiver for both energy and information, causing great interference to other nodes. In HAP, the downlink wireless power transfer may become interference to devices that do not need wireless power. Also, due to the hardware constraints, the energy receiver often has a lower sensitivity than the information receiver. For example, the information receiver could have a sensitivity of −50 or −40 dBm, while the energy receiver often has a sensitivity of −20 or −10 dBm. This means that a larger transmission power has to be used if power is to be delivered efficiently. Thus, wireless powered networks are likely to suffer from more and stronger interference.

Although there have been quite a few studies on the effect of interference on wireless powered communications, including the previous subsection, very few studies have

considered the interference generated by wireless power. In the following, the effect of interference generated by wireless power will be studied using the information rate for the PB, HAP, and SWIPT systems.

6.6.2.1 System and Assumptions

Consider the downlink of a multi-node multi-cell or a multi-cluster network. In this network, the desired node receives information from its nearest base station. If PB is used for wireless power transfer, it generates interference to this node as

$$I_B = \sum_{i=1}^{I} \sqrt{\frac{P_i}{d_i^v}} h_i x_i \alpha_i + \sum_{j=1}^{J} \sqrt{\frac{Q_j}{d_j^v}} g_j y_j \beta_j, \tag{6.81}$$

where I is the number of undesired data-transmitting base stations, P_i is their transmission power, d_i is their distance to the desired node, h_i is the fading channel gain between them, x_i is their transmitted symbol, α_i represents the asynchronization with data-transmitting base stations (they could start transmission earlier or later than the desired node), J is the number of undesired power-transmitting base stations, Q_j is their transmission power, d_j is their distance, g_j is the fading channel gain between them, w_j is their transmitted symbol, β_j represents the asynchronization with power-transferring base stations, and v is the path loss exponent. The first term in (6.81) is interference from the normal data transmission, while the second term in (6.81) is the extra interference incurred by wireless power transfer.

Without loss of generality, assume that all distances are uniformly distributed over a ring such that their PDF is

$$f_d(x) = \frac{2x}{r_h^2 - r_l^2}, \; r_l \le x \le r_h, \tag{6.82}$$

where r_h denotes the radius of the outer ring and r_l stands for the radius of the inner ring. The fading gains h_i and g_j are complex Gaussian random variables with zero-mean and variance $2\alpha^2$. M-ary phase shift keying (PSK) modulation is used such that $|x_i| = |y_j| = 1$. Assume that the frame length is T. The interfering base stations start their transmission randomly at t_0, where t_0 is uniformly distributed between 0 and T. Thus, their interfering power over the period of T is determined by $\frac{t_0}{T}$, which is uniformly distributed between 0 and 1 and represented by α_i and β_j.

Similarly, if HAP is adopted, the total interference at the desired node is

$$I_H = \sum_{i=1}^{I_1} \sqrt{\frac{P_i}{d_i^v}} h_i x_i \alpha_i + \sum_{i=I_1+1}^{I} \sqrt{\frac{Q_i}{d_i^v}} g_i y_i \beta_j, \tag{6.83}$$

where I_1 denotes the number of data-transmitting base stations among all I base stations and $I - I_1$ is the number of power-transmitting base stations.

Finally, using SWIPT, the interference seen by the desired node is

$$I_S = \sum_{i=1}^{I} \sqrt{\frac{P_i + Q_i}{d_i^v}} h_i x_i \alpha_i, \tag{6.84}$$

where the ith AP has a transmission power of $P_i + Q_i$, with P_i for information decoding and Q_i for energy harvesting. Essentially, a power-splitting receiver for SWIPT is considered.

Using these expressions, the received signal at the desired node is given by

$$y = \sqrt{\frac{P_0}{d_0^{\upsilon}}} h_0 x_0 + z, \tag{6.85}$$

where z can be replaced by I_B, I_H and I_S depending on the scheme used, P_0 is the transmission power, d_0 is the distance, h_0 is the fading gain, and x_0 is the transmitted symbol of the nearest base station. Finally, an interference-limited scenario is considered such that noise is ignored in the received signal. Also, the distance d_0 is assumed to be constant.

6.6.2.2 Average Interference Power

For the PB scheme, the average interference power can be derived from (6.67) as (Chen et al. 2017a)

$$E\{|I_B|^2\} = \frac{2\alpha^2}{3} d \left[\sum_{i=1}^{I} P_i + \sum_{j=1}^{J} Q_j \right]. \tag{6.86}$$

where $d = E\{\frac{1}{d_i^{\upsilon}}\} = E\{\frac{1}{d_j^{\upsilon}}\} = \frac{2(\ln r_h - \ln r_l)}{r_h^2 - r_l^2}$ for $\upsilon = 2$ and $d = \frac{2(r_l^{2-\upsilon} - r_h^{2-\upsilon})}{(r_h^2 - r_l^2)(\upsilon - 2)}$ for $\upsilon > 2$.

Similarly, for the HAP scheme (Chen et al. 2017a),

$$E\{|I_H|^2\} = \frac{2\alpha^2}{3} d \left[\sum_{i=1}^{I_1} P_i + \sum_{i=I_1+1}^{I} Q_i \right]. \tag{6.87}$$

Finally, for the SWIPT scheme (Chen et al. 2017a),

$$E\{|I_S|^2\} = \frac{2\alpha^2}{3} d \left[\sum_{i=1}^{I} P_i + \sum_{i=1}^{I} Q_i \right]. \tag{6.88}$$

From the above, two remarks can be made. First, by subtracting $\frac{2\alpha^2}{3} d \sum_{i=1}^{I} P_i$ from (6.86)–(6.88), the average interference power generated by PB is $\frac{2\alpha^2}{3} d \sum_{j=1}^{J} Q_j$, by HAP is $\frac{2\alpha^2}{3} d \sum_{i=I_1+1}^{I} (Q_i - P_i)$, and by SWIPT is $\frac{2\alpha^2}{3} d \sum_{i=1}^{I} Q_i$. Secondly, PB and SWIPT have the same average interference power when $J = I$. Also, PB and HAP have the same average interference power when $\sum_{i=I_1+1}^{I} P_i + \sum_{j=1}^{J} Q_j = \sum_{i=I_1+1}^{I} Q_i$. On the other hand, SWIPT always has larger average interference power than HAP.

6.6.2.3 Rate

To find the rate, the PDF of the instantaneous signal-to-interference ratio (SIR) is required. The SIR for the PB scheme can be written as $\gamma_p = \frac{W|h_0|^2}{|I_B|^2}$, where $W = \frac{P_0}{d_0^{\upsilon}} |x_0|^2$. Also, let $u_p = \sum_{i=1}^{I} \frac{P_i}{d_i^{\upsilon}} |x_i|^2 \alpha_i^2 + \sum_{j=1}^{J} \frac{Q_j}{d_j^{\upsilon}} |w_j|^2 \beta_j^2$. It is easy to show $|h_0|^2$ is an exponential random variable and $|I_B|^2$ is also an exponential random variable conditioned on u_p. Thus, the conditional PDF of γ_p given u_p can be expressed as

$$f_{\gamma_p|u_p}(z) = \frac{W u_p}{(u_p z + W)^2} = \frac{W \frac{1}{u_p}}{(z + W\frac{1}{u_p})^2}, \tag{6.89}$$

which holds from Gradshteyn and Ryzhik (2000, eq. (3.351.3)). Using (6.89) and an equation in Gradshteyn and Ryzhik (2000, eq. (4.291.15)), the conditional rate is

$$C(u_p) = \frac{W}{\ln 2}\frac{\ln u_p - \ln W}{u_p - W} = \frac{W}{\ln 2}\frac{\frac{1}{u_p}\ln\frac{W}{u_p}}{W\frac{1}{u_p} - 1}. \tag{6.90}$$

The next step is to find the PDF of u_p or $\frac{1}{u_p}$ for the unconditional rate. Approximations can be used. It is found that the inverse Gaussian distribution fits u_p the best for large values of I and J. For $\frac{1}{u_p}$, the Gamma and Weibull distributions provide good approximations. Using the Gamma approximation, the PDF of $\frac{1}{u_p}$ is

$$f_{\frac{1}{u_p}G}(t) \approx \frac{t^{k-1}}{\Gamma(k)k^\theta}e^{-\frac{t}{\theta}} \tag{6.91}$$

where $\Gamma(\cdot)$ denotes the Gamma function (Gradshteyn and Ryzhik 2000, eq. (8.310.1)), k stands for the shape parameter, and θ is the scale parameter of the Gamma distribution, and using the Weibull approximation, the PDF of $\frac{1}{u_p}$ is

$$f_{\frac{1}{u_p}W}(t) \approx \frac{p}{q}\left(\frac{t}{q}\right)^{p-1} e^{-(\frac{t}{q})^p}, \tag{6.92}$$

where p and q are the shape parameter and scale parameter of the Weibull distribution, respectively. Moment-matching gives $k\theta = E\{\frac{1}{u_p}\}$, $k^2\theta^2 + k\theta^2 = E\{\frac{1}{u_p^2}\}$, $q\Gamma(1+\frac{1}{p}) = E\{\frac{1}{u_p}\}$, $q^2\Gamma(1+\frac{2}{p}) = E\{\frac{1}{u_p^2}\}$. The moments of $\frac{1}{u_p}$ can be simulated.

Using the PDF of $\frac{1}{u_p}$, the unconditional rate for the PB scheme can be derived as (Chen et al. 2017a)

$$C_1 = \frac{1}{\Gamma(k)(\theta W)^k \ln 2}\int_0^\infty \frac{\ln t}{t-1}t^k e^{-\frac{t}{\theta W}}dt, \tag{6.93}$$

$$C_2 = \frac{p}{\ln 2(qW)^p}\int_0^\infty \frac{\ln t}{t-1}t^p e^{-(\frac{t}{qW})^p}dt, \tag{6.94}$$

which hold for the Gamma and Weibull approximations, respectively. Further, $\frac{\ln t}{1-t} \approx at^b$, where $a = 1.3$ and $b = -0.7$ from curve-fitting. Thus, using an equation from Gradshteyn and Ryzhik (2000, eq. (3.381.4)) for (6.96) and another equation from Gradshteyn and Ryzhik (2000, eq. (3.478.1)) for (6.97), they can be further simplified to (Chen et al. 2017a)

$$C_1 = \frac{a(\theta W)^{b+1}\Gamma(k+b+1)}{\Gamma(k)\ln 2}, \tag{6.95}$$

$$C_2 = \frac{a}{\ln 2}(qW)^{b+1}\Gamma\left(\frac{p+b+1}{p}\right). \tag{6.96}$$

Similar results for HAP and SWIPT schemes can also be obtained after replacing u_p by $u_h = \sum_{i=1}^{I_1}\frac{P_i}{d_i^v}|x_i|^2\alpha_i^2 + \sum_{i=I_1+1}^{I}\frac{Q_i}{d_i^v}|w_i|^2\beta_i^2$ for HAP, and $u_s = \sum_{i=1}^{I}\frac{P_i+Q_i}{d_i^v}|x_i|^2\alpha_i^2$ for SWIPT.

6.6.2.4 Numerical Examples

Next, some numerical examples are presented to illustrate the effects of interference caused by wireless power transfer. In the figures, $P_i = P = 20\ W$, $Q_j = Q = 40\ W$, $r_h = 100\ m$, $r_l = 1\ m$, and $\upsilon = 3$. Also, let $\hat{\gamma} = \frac{W}{\frac{d}{3}IP}$ be the benchmark average SIR when there is no wireless power. In SWIPT, PS is assumed.

Fig. 6.24 shows the rate versus $\hat{\gamma}$ using different approximations for the HAP. Figure 6.24a employs $I_1 = I - I_1 = 10$, while Figure 6.24b uses $I_1 = I - I_1 = 1000$. One sees from Figure 6.24 that the Gamma and Weibull approximations are very close to the simulated results, while the inverse Gaussian approximation only works when the values of I_1 and $I - I_1$ are large. It can be shown that similar conclusions hold for the PB and SWIPT schemes. They are not presented here to save space.

Figures 6.25 and 6.26 plot the rate versus $\hat{\gamma}$ for different wireless powered networks, when $I = J = 10$, $I_1 = 5$, and assuming the Gamma approximation. The case of no wireless power is obtained by setting $I = I_1$. One sees that the case without wireless power has the highest rate, as expected. However, this case has to be supported by conventional battery power for operation. One also sees that wireless power in general degrades the rate performance. In particular, PB and SWIPT have the smallest rate due to the largest interference caused, while HAP has the smallest interference and thus higher rate than PB and SWIPT. Nevertheless, the rate increases with $\hat{\gamma}$ and υ. Figure 6.27 shows the rate performance of PB for different J. One sees that, when $J = 2$, PB has a similar throughput

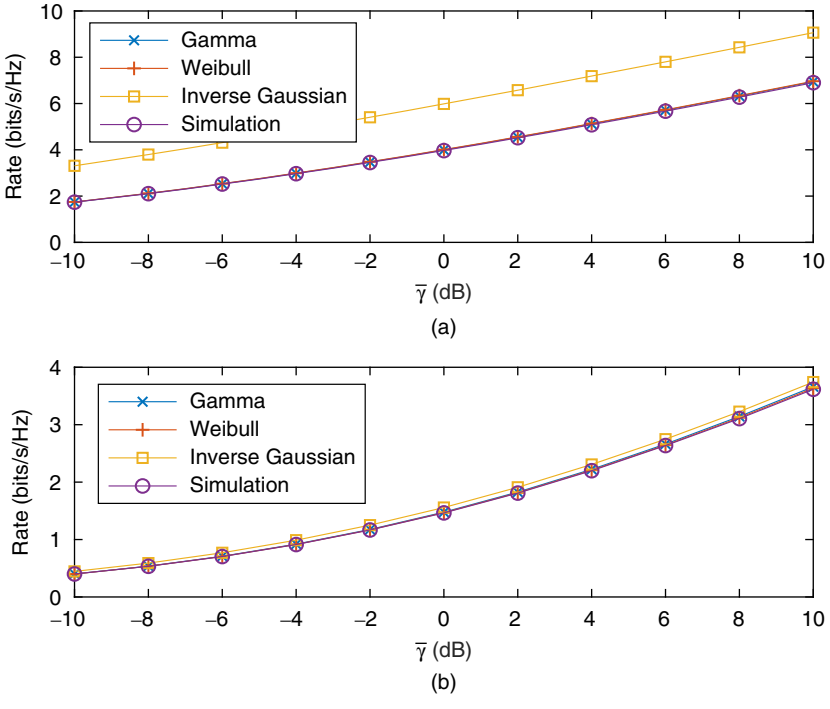

Figure 6.24 Rate of HAP versus $\hat{\gamma}$ for different approximations.

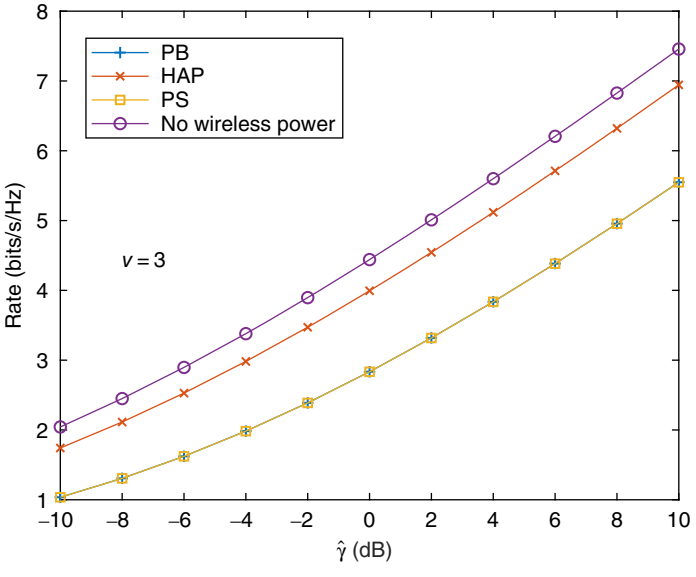

Figure 6.25 Rate versus $\hat{\gamma}$ for different wireless powered networks when $I = J = 10$ and $I_1 = 5$ for $\upsilon = 3$.

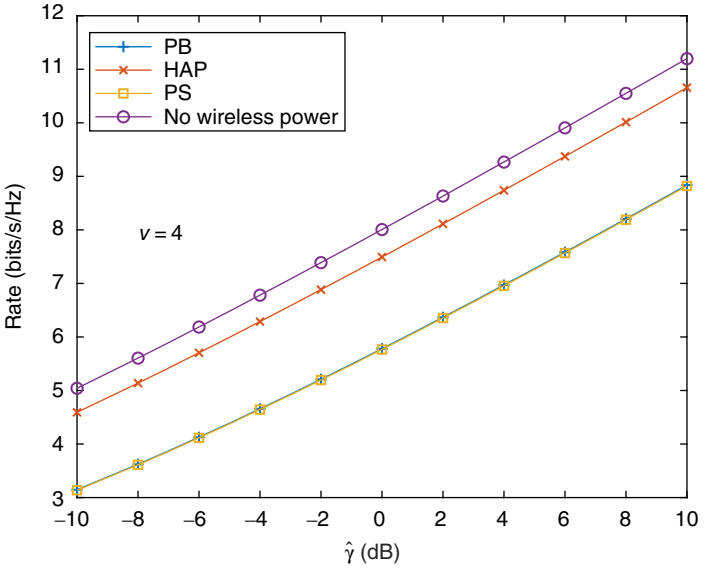

Figure 6.26 Rate versus $\hat{\gamma}$ for different wireless powered networks when $I = J = 10$ and $I_1 = 5$ for $\upsilon = 4$.

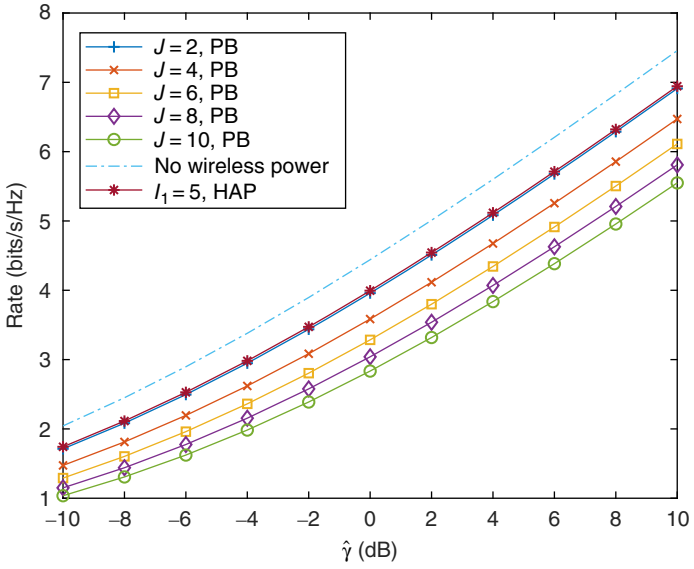

Figure 6.27 Comparison of PB using different J and HAP.

to HAP. Figure 6.28 compares different values of I_1 for HAP. A larger I_1 gives higher rate. More results on the effect of interference can be found in Chen et al. (2017a).

6.6.3 Exploitation of Interference

In the previous two subsections, the effect of interference on and caused by the wireless power has been studied. In this subsection, the interference is used as an energy source to power up the devices. In particular, nodes in the idle mode can harvest energy from peer nodes in the network that are transmitting data. Most RF energy harvesting works consider either energy harvesting from dedicated sources or energy harvesting from ambient sources. The ambient sources have great uncertainty, while the dedicated sources require extra infrastructure. In Xie et al. (2017), peer harvesting was studied, where idle nodes harvest energy from other transmitting peer nodes. This method offers a good alternative. Compared with dedicated sources, peer harvesting reuses the RF power transmitted by peer nodes to increase the lifetime of the operation. Compared with ambient sources, the transmitted signals from peer nodes in the same network are more controllable and hence have less uncertainty.

In this subsection, we analyze how long peer harvesting for a wireless network can last. In this network, multiple nodes share the same channel and transmit data in turn. When nodes are not transmitting, they will harvest energy from the transmitting nodes. The harvested energy can then be used to perform extra transmission, which can then be harvested by other nodes again. We are interested in finding out the number of extra transmissions each node can make by using the extra energy from peer harvesting.

Specifically, we consider a wireless network that has N independent nodes. These nodes access the same channel in a time-division-duplex manner by using the round-robin algorithm, where each node is assigned a time slot of T seconds so that all

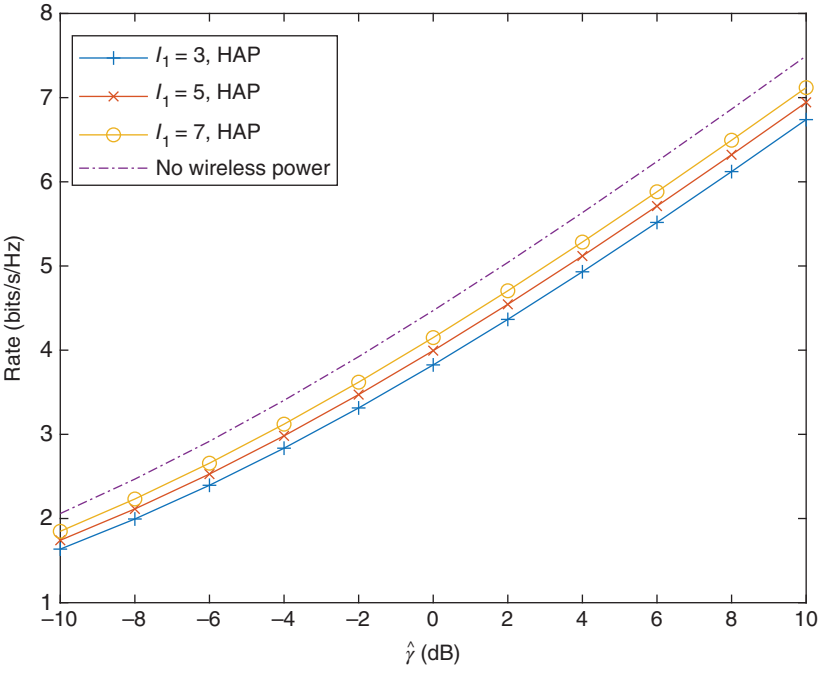

Figure 6.28 Comparison of different I_1 for HAP.

nodes finish their transmission in NT seconds. Without loss of generality, we assume that the nodes transmit in the order of $1, 2, \cdots, N$. Also, assume that all the nodes have data to transmit during their assigned time slots and only transmit during their assigned slots. Each transmission has a fixed transmission power of P. The initial energy available at each node before any transmission starts is assumed to be E_0. Essentially, it is interesting to find out how many transmissions the total energy of NE_0 can be used for until all nodes die down due to insufficient energy.

Denote E_{ki} as the initial energy at the ith node before the kth round of transmission starts. Using the above assumptions, one can derive the energy matrix and present it as

$$\mathbf{E}_k = \begin{bmatrix} -PT\alpha_{k1} & \frac{\eta PT|h_{12k}|^2}{d_{12k}^v}\alpha_{k1} & \cdots & \frac{\eta PT|h_{1Nk}|^2}{d_{1Nk}^v}\alpha_{k1} \\ \frac{\eta PT|h_{21k}|^2}{d_{21k}^v}\alpha_{k2} & -PT\alpha_{k2} & \cdots & \frac{\eta PT|h_{2Nk}|^2}{d_{2Nk}^v}\alpha_{k2} \\ \vdots & \vdots & \ddots & \vdots \\ \frac{\eta PT|h_{N1k}|^2}{d_{N1k}^v}\alpha_{kN} & \frac{\eta PT|h_{N2k}|^2}{d_{N2k}^v}\alpha_{kN} & \cdots & -PT\alpha_{kN} \end{bmatrix} \tag{6.97}$$

where a plus sign of the element indicates energy harvesting, a minus sign of the element indicates energy consumption, and P and T, respectively, are the transmission power and the transmission time of the node giving the energy consumption of PT. Importantly, the transmission indicator is given by

$$\alpha_{ki} = \begin{cases} 1, & E_{ki} > PT, \\ 0, & E_{ki} < PT, \end{cases} \tag{6.98}$$

so that the ith node only transmits in the kth round if its energy is larger than PT and otherwise it does not transmit, η is the conversion efficiency of the energy harvester as discussed in Chapter 3, h_{ijk} is the fading coefficient between the ith node and the jth node in the kth round, d_{ijk} is their distance, v is the path loss exponent, and $i = 1, 2, \cdots, N$ represent different nodes. The fading coefficients are assumed independent for different values of i and j. Rayleigh fading channels are used so that the fading coefficient is a circularly symmetric complex Gaussian random variable with mean 0 and variance $2\sigma^2$.

In the energy matrix, the first row gives the energy change after node 1 finishes its time slot. If node 1 has enough energy to transmit, node 1 will have an energy consumption of PT while other nodes will harvest an energy of $\frac{\eta PT|h_{1ik}|^2}{d_{1ik}^v}$ from node 1's transmission, $i = 2, 3, \cdots, N$. If node 1 does not transmit, the energy changes will be zero at all nodes in this case. Assume $E_0 = K * PT$. After K rounds, the extra energy harvested at the ith node is given by

$$E_{(K+1)i} = \sum_{l=1}^{K} \sum_{j=1, j\neq i}^{N} \frac{\eta PT|h_{jil}|^2}{d_{jil}^v}. \tag{6.99}$$

This energy harvested from peer nodes during their transmissions in the K rounds can be used to perform extra data transmissions. The larger the value of $E_{(K+1)i}$, the more extra transmissions the ith node can perform. Thus, the number of extra transmissions each node makes indicates how long the lifetime of the network can be.

Assume that m extra transmissions can be made. The energy matrix of the $(K + m - 1)$th round can be derived from (6.97) by replacing k with $K + m - 1$ to give

$$\mathbf{E}_{(K+m-1)} = \begin{bmatrix} -PT\alpha_{(K+m-1)1} & \cdots & \frac{\eta PT|h_{1N(K+m-1)}|^2}{d_{1N(K+m-1)}^v}\alpha_{(K+m-1)1} \\ \frac{\eta PT|h_{21(K+m-1)}|^2}{d_{21(K+m-1)}^v}\alpha_{(K+m-1)2} & \cdots & \frac{\eta PT|h_{2N(K+m-1)}|^2}{d_{2N(K+m-1)}^v}\alpha_{(K+m-1)2} \\ \vdots & \ddots & \vdots \\ \frac{\eta PT|h_{N1(K+m-1)}|^2}{d_{N1(K+m-1)}^v}\alpha_{(K+m-1)N} & \cdots & -PT\alpha_{(K+m-1)N} \end{bmatrix}. \tag{6.100}$$

From (6.100), by summing up its ith column and using iteration, the residual energy after the $(K + m - 1)$th round or the initial energy of the $(K + m)$th round can be derived as

$$\begin{aligned} E_{(k+m)i} = E_{(K+1)i} &- PT \sum_{p=1}^{m-1} \alpha_{(K+p)i} \\ &+ \sum_{p=1}^{m-1} \sum_{j=1, j\neq i}^{N} \frac{\eta PT|h_{ji(K+p)}|^2}{d_{ji(K+p)}^v}\alpha_{(K+p)j}, \end{aligned} \tag{6.101}$$

where $i = 1, 2, \cdots, N$. To allow for the transmission of m extra rounds, one must have $E_{(k+p)i} > PT$ for $p = 1, 2, \cdots, m$ and $i = 1, 2, \cdots, N$. Thus, the probability that m extra rounds of transmission can be made is determined by

$$P_m = Pr\{E_{(k+p)i} > PT, p = 1, 2, \cdots, m, i = 1, 2, \cdots, N\}. \tag{6.102}$$

In (6.102), the random fading coefficient makes the event uncertain. One has from (6.102)

$$P_m = \prod_{i=1}^{N} Pr\{G_{(K+1)i} > PT, \tag{6.103}$$

$$G_{(K+1)i} + G_{(K+2)i} > 2PT, \cdots, \sum_{p=1}^{m} G_{(K+p)i} > mPT\},$$

where

$$G_{(K+1)i} = \sum_{l=1}^{K} \sum_{j=1, j\neq i}^{N} \frac{\eta PT|h_{jil}|^2}{d_{jil}^{v}} \tag{6.104}$$

$$G_{(K+p)i} = \sum_{j=1, j\neq i}^{N} \frac{\eta PT|h_{ji(K+p-1)}|^2}{d_{ji(K+p-1)}^{v}}, p = 2, \cdots, m. \tag{6.105}$$

Thus, m is a discrete random variable with probability mass function given by (6.103). We are interested in the distribution of this random variable. A general expression of the distribution is not possible but for small values of m, it is possible. In particular, when $m = 1$, one has (Chen et al. 2018)

$$P_1 = \prod_{i=1}^{N} \left[\sum_{j_1=1, j_1\notin\phi_i}^{NK} \beta_{j_1 i(K+1)} e^{-\lambda_{j_1 i(K+1)} PT} \right]. \tag{6.106}$$

where $\lambda_{j_1 i(K+1)} = \frac{d_{j_1 i}^{v}}{2\sigma^2 \eta PT}$, $\beta_{j_1 i(K+1)} = \prod_{l_1=1, l_1\neq j_1}^{NK} \frac{\lambda_{l_1 i(K+1)}}{\lambda_{l_1 i(K+1)} - \lambda_{j_1 i(K+1)}}$, and the distances $d_{1i}, d_{2i}, \cdots, d_{(NK)i}$ correspond to $d_{1i1}, d_{2i1}, \cdots, d_{NiK}$, respectively, and we have stacked the two summations in (6.106) into one summation and in the stacked summation there are $(N-1)K$ terms, as ϕ_i contains the N terms excluded in the second summation of (6.106).

When $m = 2$, one has (Chen et al. 2018)

$$P_2 = \prod_{i=1}^{N} \{ \sum_{j_1=1, j_1\notin\phi_i}^{NK} \beta_{j_1 i(K+1)} e^{-\lambda_{j_1 i(K+1)} 2PT}$$
$$\times [1 + \sum_{j_2=1, j_2\neq i}^{N} \frac{\beta_{j_2 i(K+2)} (1 - e^{PT(\lambda_{j_1 i(K+1)} - \lambda_{j_2 i(K+2)})})}{\frac{\lambda_{j_2 i(K+2)}}{\lambda_{j_1 i(K+1)}} - 1}]\}. \tag{6.107}$$

where $\lambda_{j_2 i(K+2)} = \frac{d_{j_2 i(K+1)}^{v}}{2\sigma^2 \eta PT}$, $\beta_{j_2 i(K+2)} = \prod_{l_2=1, l_2\neq j_2}^{N} \frac{\lambda_{l_2 i(K+2)}}{\lambda_{l_2 i(K+2)} - \lambda_{j_2 i(K+2)}}$, $\lambda_{j_3 i(K+3)} = \frac{d_{j_3 i(K+2)}^{v}}{2\sigma^2 \eta PT}$, and $\beta_{j_3 i(K+3)} = \prod_{l_3=1, l_2\neq j_3}^{N} \frac{\lambda_{l_3 i(K+3)}}{\lambda_{l_3 i(K+3)} - \lambda_{j_3 i(K+3)}}$.

When $m = 3$, one has (Chen et al. 2018)

$$P_3 = \prod_{i=1}^{N} [I_1 + I_2 + I_3 + I_4] \tag{6.108}$$

where

$$I_1 = \sum_{j_1=1, j_1\notin\phi_i}^{NK} \beta_{j_1 i(K+1)} e^{-\lambda_{j_1 i(K+1)} 3PT}$$

$$I_2 = \sum_{j_1=1, j_1 \notin \phi_i}^{NK} \sum_{j_2=1, j_2 \neq i}^{N} \frac{\beta_{j_1 i(K+1)} \beta_{j_2 i(K+2)}}{\frac{\lambda_{j_2 i(K+2)}}{\lambda_{j_1 i(K+1)}} - 1} (e^{-\lambda_{j_1 i(K+1)} 3PT} - e^{-\lambda_{j_2 i(K+2)} 3PT})$$

$$I_3 = \sum_{j_1=1, j_1 \notin \phi_i}^{NK} \sum_{j_2=1, j_2 \neq i}^{N} \sum_{j_3=1, j_3 \neq i}^{N} \beta_{j_1 i(K+1)} \beta_{j_2 i(K+2)} \beta_{j_3 i(K+3)}$$
$$\times \left[\frac{e^{-\lambda_{j_1 i(K+1)} 3PT} - e^{-(\lambda_{j_1 i(K+1)} 2PT + \lambda_{j_2 i(K+2)} PT)}}{\lambda_{j_2 i(K+2)} - \lambda_{j_1 i(K+1)}} - \frac{e^{-\lambda_{j_1 i(K+1)} 3PT} - e^{-(\lambda_{j_1 i(K+1)} 2PT + \lambda_{j_3 i(K+3)} PT)}}{\lambda_{j_3 i(K+3)} - \lambda_{j_1 i(K+1)}} \right]$$

$$I_4 = \sum_{j_1=1, j_1 \notin \phi_i}^{NK} \sum_{j_2=1, j_2 \neq i}^{N} \sum_{j_3=1, j_3 \neq i}^{N} \beta_{j_1 i(K+1)} \beta_{j_2 i(K+2)} \beta_{j_3 i(K+3)}$$
$$\times \frac{e^{-\lambda_{j_2 i(K+2)} 3PT} - e^{-(\lambda_{j_2 i(K+2)} 2PT + \lambda_{j_3 i(K+3)} PT)}}{\lambda_{j_3 i(K+3)} - \lambda_{j_1 i(K+1)}} \frac{e^{\lambda_{j_2 i(K+2)} - \lambda_{j_1 i(K+1)} 2PT} - 1}{\lambda_{j_2 i(K+2)} - \lambda_{j_1 i(K+1)}}.$$

A similar method can be used to derive results for $m = 4$ and so on. However, the expressions are becoming more and more complicated as m increases. Also, the CDF of m can be calculated as $F_m(x) = \sum_{m=1}^{x} P_m$. The above results assume that there is only one node transmitting in each time slot. If more than one node is transmitting at the same time, such as two-way relaying or non-orthogonal multiple access, similar results can be obtained by replacing $j \neq i$ with $j \neq \psi_i$, where ψ_i is the set of nodes that transmit at the same time as the ith node. In this case, there will be less harvested energy due to simultaneous transmissions but the total time of each round will be reduced to increase the throughput.

Next, numerical examples are presented to show the number of extra transmissions. In these examples, three typical network topologies are considered: all nodes are evenly distributed over a line with length L and fixed positions; all nodes are randomly distributed over a line with length L; and all nodes are randomly distributed over a disc with radius R. The line models may be found in vehicular communications on a highway, while the disc model may be found in cellular communications. Since it is difficult to obtain analytical results for large values of m, we use computer simulation. In the simulation, we set $\eta = 0.5$, $PT = 1$, $2\sigma^2 = 1$, and other parameters are given in the figures.

Figures 6.29 and 6.30 show P_m versus m for different system settings. One sees that the probability of having extra rounds of transmission decreases when m increases. This is expected, as all the energy will eventually be consumed such that it becomes less and less possible to perform extra transmissions. Comparing the three different topologies in Figure 6.29, one sees that the random line has the highest probability, followed by the fixed line and then the random disc. This implies that a network with nodes randomly distributed over a line can harvest more energy and thus can have a longer operation time than those randomly distributed over a disc or evenly distributed over a line. Comparing Figure 6.29 with Figure 6.30, one also sees that a larger value of K allows for higher probability of extra transmission. This means that one can increase the operational time by allocating more initial energy.

Figure 6.31 shows P_m versus m when two nodes transmit at the same time in each time slot. In this case, the fixed line becomes the worst case, while the random line is still the best case. The data rate increases by using simultaneous transmission and the energy that can be harvested in each transmission also increases but the number

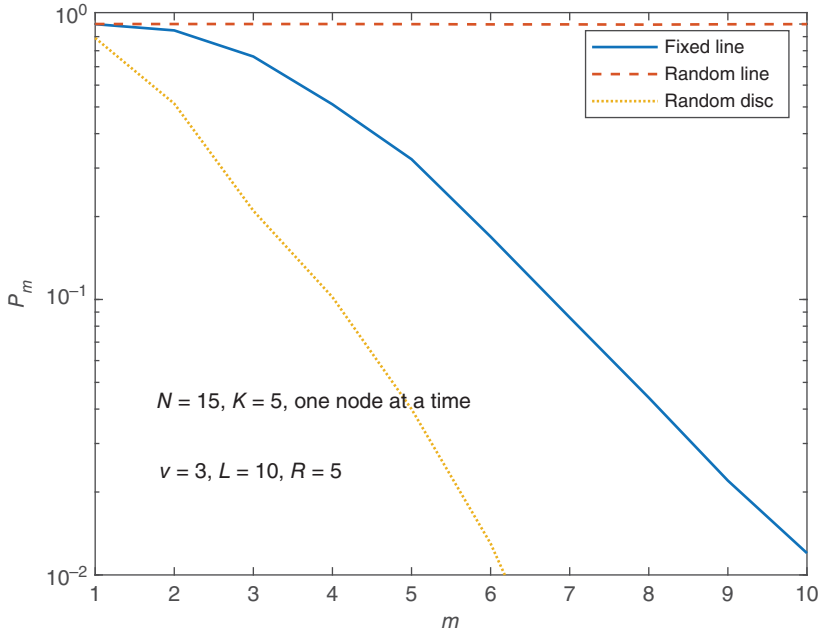

Figure 6.29 P_m versus m for different topologies when only one node transmits in each time slot using round-robin.

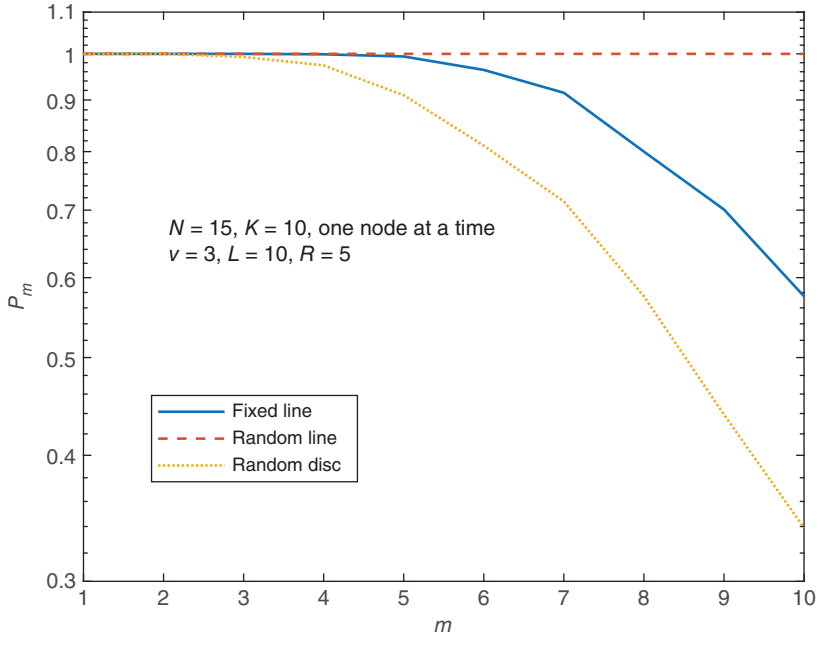

Figure 6.30 P_m versus m for different topologies when only one node transmits in each time slot using round-robin.

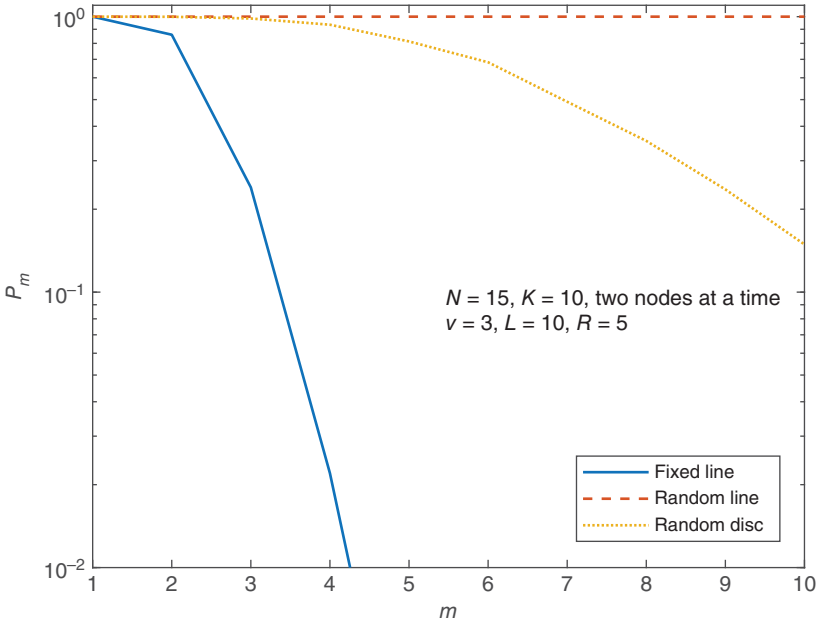

Figure 6.31 P_m versus m for different topologies when two nodes transmit data simultaneously in each time slot using round-robin.

of transmissions in each round will be reduced. This is different from the single-node transmission case. Figure 6.32 shows the average value of m versus the number of nodes N. Indeed, on average the number of extra transmissions increases with the number of nodes. This increase is very slow at the beginning but then dramatic after a threshold before it slows down again. The random line has the highest average, followed by the random disc and the fixed line.

Figure 6.33 focuses on the random line case for different system parameters. In this case, the length of the line has been increased to $L = 30\,m$. One sees that the probability of extra transmission is very sensitive to K. A decrease of K from 10 to 5 leads to a dramatic drop in probability. The probability also decreases when N decreases from 15 to 10, as less energy can be harvested in each round due to less transmitting nodes. This is also observed from Figure 6.32. Finally, comparing one-node transmission with two-node transmission, the probability of extra transmission is smaller in two-node transmission. This implies that the effect of having less transmissions is larger than the effect of having more energy harvested in each transmission. More details on the derivation can be found in Chen et al. (2018).

6.6.4 Multiple Antennas

In wireless communications, multiple-input-multiple-output (MIMO) has been proven as an effective means of achieving high data rate. Similar ideas can also be applied to wireless powered communications. Consider the use of multiple antennas in SWIPT (Zhang and Ho 2013). In this case, the transmitter uses M antennas, and the receiver uses N antennas. The received signal is used for both energy harvesting and information

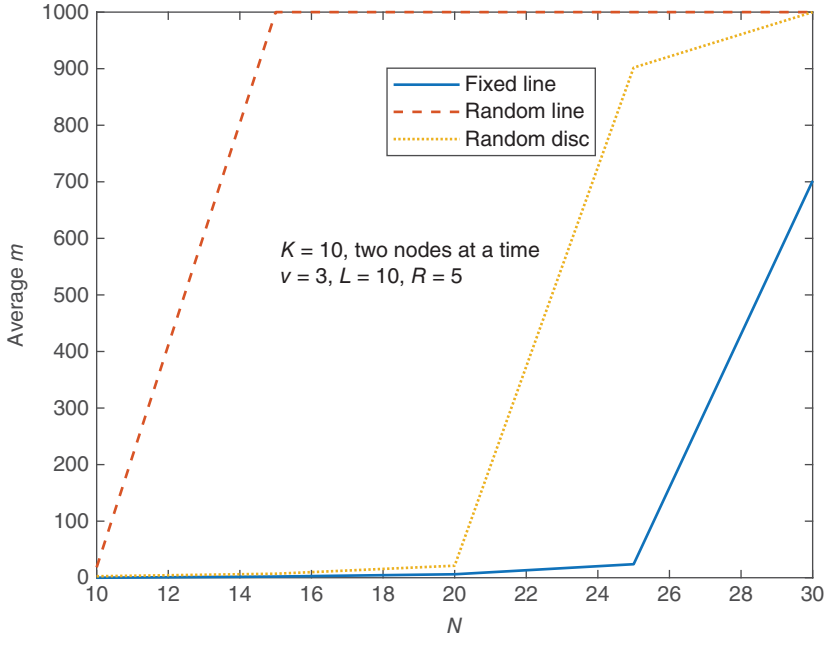

Figure 6.32 The average value of m for different topologies when two nodes transmit data simultaneously in each time slot using round-robin.

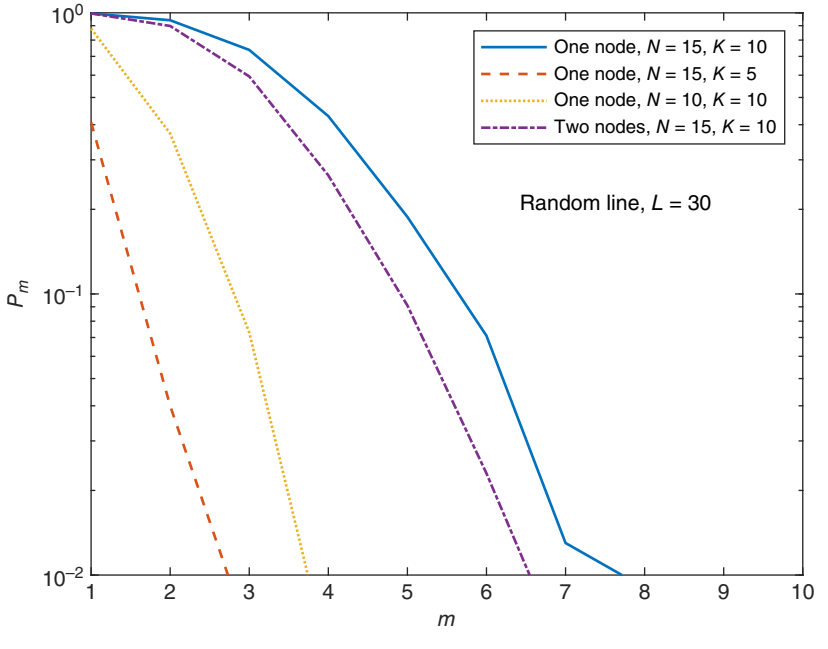

Figure 6.33 Comparison of different transmission strategies.

decoding. The channel matrix between the transmitter and the receiver is denoted by $\mathbf{H}$, which is a $N \times M$ matrix. The received signal is thus denoted as

$$\mathbf{y} = \mathbf{Hs} + \mathbf{z} \tag{6.109}$$

where $\mathbf{y}$ is a $N \times 1$ vector representing received signals on all antennas, $\mathbf{s}$ is a $M \times 1$ vector representing the transmitted signals on all antennas, and $\mathbf{z}$ is a $N \times 1$ vector representing AWGN. Denote $\mathbf{S} = E[\mathbf{ss}^H]$ as the covariance matrix of $\mathbf{s}$, where $E[\cdot]$ is the expectation operation and H is the conjugate transpose operation.

If the received signal in (6.109) is used for energy harvesting, the harvested power (energy normalized by the symbol interval) is given by

$$Q = \eta E[||\mathbf{Hs}||^2] = \eta tr(\mathbf{HSH}^H) \tag{6.110}$$

where $tr(\cdot)$ is the trace operation and η is the conversion efficiency.

On the other hand, if the received signal in (6.109) is used for information decoding, the achievable information rate is

$$R = \log|\mathbf{I} + \mathbf{HSH}^H| \tag{6.111}$$

where $\mathbf{I}$ is the $M \times M$ identity matrix and $|\cdot|$ is the determinant operation.

Similar to the single antenna case, the optimization problem here is to maximize both Q and R, which leads to a tradeoff between energy and information. If TS is used, this tradeoff is represented by the rate-energy function as

$$\begin{aligned} &C(R,Q) = \{Q \le \eta\alpha \cdot tr(\mathbf{HS}_E\mathbf{H}^H), R \le (1-\alpha)\log|\mathbf{I} + \mathbf{HS}_I\mathbf{H}^H|, \\ &tr(\mathbf{S}_I) < P_s, tr(\mathbf{S}_E) < P_s, \mathbf{S}_I \ge 0, \mathbf{S}_E \ge 0\} \end{aligned} \tag{6.112}$$

where $tr(\mathbf{S}_I)$ is the transmission power during information decoding and $tr\{\mathbf{S}_E\}$ is the transmission power during energy harvesting. Comparing (6.112) and (6.11), one sees that they are very similar to each other.

If PS is used, the rate-energy function becomes

$$\begin{aligned} &C(R,Q) = \{Q \le \eta \cdot tr(\mathbf{\Lambda}_1\mathbf{HSH}^H), R \le \log|\mathbf{I} + \mathbf{\Lambda}_2{}^{1/2}\mathbf{HSH}^H\mathbf{\Lambda}_2{}^{1/2}|, \\ &tr(\mathbf{S}) < P_s, \mathbf{S} \ge 0\} \end{aligned} \tag{6.113}$$

where $\mathbf{\Lambda}_1 = diag(\rho_1, \cdots, \rho_N)$ is a diagonal matrix that has all the PS factors of the receiving antennas in the diagonal line, and $\mathbf{\Lambda}_2 = diag(\upsilon_1, \cdots, \upsilon_N)$, $\upsilon_n = \frac{1-\rho_n}{(1-\rho_n)2\sigma_a^2 + 2\sigma_d^2}$, and $2\sigma_a^2$ and $2\sigma_d^2$ are the noise power for the RF antenna and the RF-to-baseband conversion defined as before.

Using (6.112) and (6.113), further optimizations are possible. For example, one can maximize Q subject to a constraint on R, or maximize R subject to a constraint on Q. The parameters to be optimized could be P_s, α, ρ, M, N, and so on. Alternatively, energy beamforming and information beamforming can also be used for MIMO systems (Liu et al. 2014b). In this case, $\mathbf{s}$ will be replaced by $\mathbf{Us}$ and $\mathbf{H}$ will be replaced by $\mathbf{VH}$, where $\mathbf{U}$ and $\mathbf{V}$ are the precoding and decoding matrices at the transmitter and the receiver, respectively. Then, $\mathbf{U}$ and $\mathbf{V}$ can be jointly maximized with P_s, α, ρ, M, and N, leading to even more variants.

These two rate-energy functions are the basis of all these optimization studies in the literature. In fact, the tradeoff proposed in Varshney (2008) and Grover and Sahai (2010) are the starting points of all these studies.

6.7 An Example: Wireless Powered Sensor Networks

Wireless sensor networks (WSNs) have been widely used in our daily lives, such as in smart cities, asset monitoring, home automation, and logistics. When Internet of Things networks are deployed, they will become more popular, as many applications will have embedded sensing devices installed for various purposes (Raza et al. 2017).

As WSNs spread and scale up, one issue is becoming more and more serious. Most existing sensors rely on either battery or mains connection for power supply. For mobile applications, battery is actually the only choice. However, all batteries have a limited lifetime. When the battery runs out, it has to be replaced, or the whole network could break down. In a sensor network with hundreds or even thousands of sensors, this is almost a mission impossible, not to mention that some sensors could be embedded in buildings or human bodies such that their replacement incurs a huge amount of extra cost or pain.

Meanwhile most sensor networks are used for low-power applications, such as environment monitoring, where sensors only need to send data occasionally with very low duty cycles. Their power consumption is often on the scale of milliwatts or even microwatts. On the other hand, studies have shown that even the ambient RF energy can provide a harvested power on the scale of milliwatts or microwatts (Azmat et al. 2016). Thus, wireless power and wireless sensor networks are a perfect match (Xie et al. 2013). Indeed, most current wireless power designs are for sensor networks or other low-power applications.

For example, in Tong et al. (2010), commercially available wireless power products were used to test the efficiency of wireless power transfer for sensor networks. The results revealed that the efficiency is quite low so that custom-made hardware may be necessary to supply wireless power for sensor networks. In Peng et al. (2010) a mobile robot was used to charge a sensor network. The optimal scheduling and the optimal path of this robot were studied to prolong the lifetime of the network. Their results showed that wireless power can improve the network lifetime, but the power transfer efficiency is still an issue that needs to be resolved for better results. The power transfer efficiency of different harvesters has been extensively studied in Chapter 3. In a wider context, Erol-Kantarci and Touftah (2012) studied a rechargeable WSN used for smart grid monitoring. This scheme is similar to the PB wireless powered networks, where a few dedicated power transmitters are installed to supply power for the sensor network. Kamalinejad et al. (2015) reviewed and studied the use of wireless power in the Internet of Things by focusing on the extended network lifetime. Some future challenges have also been discussed.

There are many other applications of sensor networks using wireless power. Interested readers are referred to Sudevalayam and Kulkarni (2011) and Lu et al. (2015) for a more complete review of wireless powered sensing.

6.8 Summary

This chapter has mainly focused on wireless powered communications. Three different types of wireless powered communications have been discussed: SWIPT; HAP; and PB. They have different pros and cons. For PB, it simplifies the fundamental tradeoff between

energy and information, but it incurs a large amount of extra infrastructure cost. This extra infrastructure cost may not be desirable for most existing applications and hence, it is more suitable for future networks. For SWIPT and HAP, they are relatively easy to implement with little infrastructure upgrade but the implementation involves complicated protocol design problems. They are more suitable for existing networks that require additional wireless power capability, as the changes will be mainly on protocols rather than network infrastructure.

Several important research issues on wireless powered communications have also been reviewed. It has been emphasized that most of these research problems start from the tradeoff between energy and information. In most cases, the amount of harvested energy and the information rate can be derived, based on which different system parameters can be optimized. However, in these cases, the power that can be supplied by far-field wireless transfer is still low. Thus, an example of using low wireless power in sensor networks has been examined.